Late Cenozoic transtensional deformation along the Chenghai fault zone and its constraint on micro-block clockwise rotation in southeastern Tibetan Plateau

zhonghai wu[1], xiaolong Huang[2], xiaojin Huang[3], Feng Liu[4], and kungang Wu[2]

[1]The Institute of Geomechanics, Chinese Academy of Geological Sciences
[2]Institute of Geomechanics, Chinese academy of geological sciences
[3]School of Civil Engineering and ArchitectureWuyi University
[4]Institute of Geomechanics, Chinese Academy of Geological Sciences

November 23, 2022

Abstract

The Chenghai fault zone, an important part of the Dali fault system, is instrumental in comprehending the crustal deformation of the southeastern margin of the Tibetan Plateau. Detailed remote sensing interpretation and field mapping are used to study the geometry and kinematic characteristics of this fault. The results show that the Chenghai fault zone extends up to 200 km from Jinguan to the south end of the Midu basin, and it truncated and inherited the trace of the Red River fault on the east side of the Midu basin. Furthermore, it is an oblique-slip fault with both normal and sinistral strike-slip component, and the normal component is more significant. The transtensional activity of this fault may have started in the Early Pliocene (5–6 Ma). The average maximum dip-slip rate can be 0.37–0.57 mm/yr, and the maximum left-slip rate is 0.83–1.20 mm/yr. The clockwise rotation of the Dali block resulted in the Z-shaped Dali fault system and the Chenghai fault zone. Moreover, the difference of angular velocity between the inner and the outer arcuate belts divided by the Litang–Dali–Ruili fault system leads to the clockwise rotation of the Dali block.

Late Cenozoic transtensional deformation along the Chenghai fault zone and its constraint on micro-block clockwise rotation in southeastern Tibetan Plateau

Xiaolong Huang [1*], Zhonghai Wu [1*], Xiaojin Huang[2], Feng Liu[1], Kungang Wu[1]

[1] Key Laboratory of Neotectonic Movement & Geohazard, Institute of Geomechanics, Chinese Academy of Geological Sciences, Beijing, 100081, China

[2] Research Institute for Smart Cities, Shenzhen University, Shenzhen, 518060, China

* Corresponding author:

Zhonghai Wu, Institute of Geomechanics, Chinese academy of geological sciences, Beijing, China 100081. E–mail address: wuzhonghai@geomech.ac.cn.

Xiaolong Huang, Institute of Geomechanics, Chinese academy of geological sciences, Beijing, China 100081. E–mail address: tinyloong@163.com.

Key Points:

- The Chenghai fault zone is an oblique–slip fault and the normal component is more significant.
- The transtensional activity along Chenghai fault zone may have started in the Early Pliocene about 5–6 Ma.
- The transtensional deformation of the Chenghai fault zone is the result of micro-block clockwise rotation in southeastern Tibetan Plateau.

Abstract

The Chenghai fault zone, an important part of the Dali fault system, is instrumental in comprehending the crustal deformation of the southeastern margin of the Tibetan Plateau. Detailed remote sensing interpretation and field mapping are used to study the geometry and kinematic characteristics of this fault. The results show that the Chenghai fault zone extends up to 200 km from Jinguan to the south end of the Midu basin, and it truncated and inherited the trace of the Red River fault on the east side of the Midu basin. Furthermore, it is an oblique-slip fault with both normal and sinistral strike-slip component, and the normal component is more significant. The transtensional activity of this fault may have started in the Early Pliocene (5–6 Ma). The average maximum dip-slip rate can be 0.37–0.57 mm/yr, and the maximum left-slip rate is 0.83–1.20 mm/yr. The clockwise rotation of the Dali block resulted in the Z-shaped Dali fault system and the Chenghai fault zone. Moreover, the difference of angular velocity between the inner and the outer arcuate belts divided by the Litang–Dali–Ruili fault system leads to the clockwise rotation of the Dali block.

1 Introduction

The collision between the Indian and Eurasian plates in the early Cenozoic and the wedge effect after the collision not only formed several active mountain systems in the Himalayas and Central Asia but also formed a series of large-scale active strike-slip faults, which had a significant impact on the geomorphic pattern and environmental evolution of the surrounding areas (Molnar et al., 1975, 1993; Tapponnier et al., 2001; Taylor & Yin, 2009). Several models have been proposed to explain the deformation of the southeastern margin of the Tibetan Plateau, such as (1) lateral extrusion of rigid blocks, in which deformation is mainly localized along strike-slip faults that bound the blocks (Molnar, 1975; Tapponnier et al., 1982, 1990, 2001); (2)

rotational deformation mode with limited extrusion, in which deformation is mainly regulated by rotation deformation between blocks (Molnar and Lyoncaent, 1989; England and Molnar, 1990; Holt et al., 1991; Xu et al., 2003; Schoenbohm et al., 2006); (3) continuous deformation, in which deformation is achieved through creep deformation of crust/lithosphere (England and Houseman, 1986; Dewey et al., 1988; Houseman and England, 1993; Royden et al., 1997; Clark et al., 2000; Copley, 2008; Bai et al., 2010); and (4) clockwise rotation deformation mode (Wang et al., 1998), which assumes that the crustal deformation pattern on the southeastern margin of the Tibetan Plateau is mainly based on the Yushu–Xianshuihe–Xiaojiang–Dien Bien Phu fault zone as the east boundary and the clockwise rotation deformation around the eastern Himalayan tectonic knot. GPS observations further confirmed the existence of rotational deformation (Chen et al., 2000; Zhang et al., 2004; Shen et al., 2005). However, with the continuous emergence and discovery of new data, especially the research on the main active faults in the area and geophysical and GPS observations, among others, the existing models can no longer fully explain the current crustal deformation in the southeastern margin of the Tibetan Plateau.

The southeastern margin of the Tibetan Plateau (SEMTP) is featured by a set of curved strike-slip faults that develop and evolve around the eastern Himalayan syntaxis (Allen et al., 1991; Tapponnier et al., 1986; Wang and Burchfiel, 1997; Wang et al., 1998). The Xianshuihe–Xiaojiang fault and its SW extension to the Dien Bien Phu fault beyond the Red River fault zone form the outer ring (Wang et al., 1998), whereas the Litang, Wanding, and Nantinghe faults constitute the inner ring (Wu et al., 2015; Shi et al., 2018). The Red River fault zone cuts through this curved strike-slip fault zone composed of the Xianshuihe, Xiaojiang and Dien Bien Phu fault. Despite the predominance of strike-slip faulting in this region, a remarkable extensional structure develops in the inner zone where the Litang, Nantinghe, and Red River faults intersect and become an earthquake-prone zone (Wang et al., 1998; Anne and Manuel, 2005; Fan et al., 2006) (Figure 1). This extensional zone, that is, the Dali fault depression zone, hosted several large-to-moderate earthquakes (Figure 2). However, the kinematic relationship among these active structures is unclear and has become an intensely debated subject.

Based on the different deformation models of the southeast Tibetan Plateau, numerous dynamic mechanisms have been suggested to explain the deformation in the Dali fault system. Allen et al. (1984) suggested that the extensional deformation in the Dali fault system resulted from the tip extension of the Red River fault; Wang et al. (1998) proposed that it was related to the clockwise rotation of micro-fault blocks along with the tip extension of concomitant strike-slip faults; Wu et al. (2009, 2015) attributed it to a clockwise rotational movement of the Litang–Dali–Ruili arc structure zone. The difference in these explanations is a direct deduction of the poor and crude understanding of the geometric and kinematic features of the Dali fault system.

This paper focuses on the Chenghai fault zone, which is the eastern boundary fault of the Dali fault system (Wang et al., 1998), extending about 200 km from Yongsheng to Midu, as clearly revealed by satellite images. The Chenghai fault zone has been briefly introduced in the study of the Red River fault and other large-scale fault systems in the southeastern Tibetan Plateau. Moreover, it is known to be an active left-slip fault with normal fault components (Wang et al., 1998), and it terminates on the eastern side of the Red River fault (Socquet and Pubellier, 2005). However, Schoenbohm et al. (2006) proposed that the Red River fault is truncated and offsets ~7 km left laterally by the Chenghai fault zone in Midu basin. In addition, several segments of the Chenghai fault zone have been studied, indicating that the fault has a complex geometrical structure, along with a remarkable normal displacement (Li and Jin, 1990; Fan et al., 2006; Luo et al., 2015; Huang et al., 2016). However, the lack of detailed fault mapping leads to a poor understanding of the exact structure and motion sense of the whole Chenghai fault zone at present, and the interaction between the Red River fault and Chenghai fault zone is not clear.

In this paper, new field observations and evidence for the structure and motion sense of the Chenghai fault zone are presented, as along with its relationship with the Red River fault evaluated through detailed mapping of the Chenghai fault zone. Furthermore, the dynamic progressive mechanism of this fault and its relationship with the crustal deformation in the SEMTP are discussed.

2 Geological setting

2.1 Neotectonics and seismicity

As the motion of the Red River fault changed into right-lateral shearing in the Pliocene (Lacassin et al., 1998; Replumaz et al., 2001), a series NW, NE, and N–S striking faults are widely distributed in the Dali block (e.g., Wang et al., 1998; Fan et al., 2006; Wu et al., 2009; Huang et al., 2018), which are grouped into the Dali fault system (Wang et al., 1998) (Figure 2). Faults in the Dali fault system can be divided into four fracture systems. The Chenghai fault zone is an oblique normal sinistral fault (Li and Jin, 1990; Wang et al., 1998), which has a 0.5–0.6mm/yr dip-slip rate during the Holocene at the northern tip of this fault (Huang et al., 2018). The Lijiang–Dali graben system is a Z-shaped zone that consists of a series of N-striking and NW-striking extensional faults from Daju to Dali. They are arcuate Haba–Yulong Snow Mountain normal fault (Wu et al., 2009), NNE-striking Heqing normal fault (Wang et al., 1998), NE-striking Heqing–Eryuan oblique fault with both normal and sinistral strike-slip faults (Tang et al., 2010), and Eastern Piedmont normal fault of Diancang Mountain after a significant

Holocene activity (Mao et al., 2003). The Tongdian–Weishan fault zone is a dextral strike-slip fault, which has a 1.25 mm/yr average dextral strike-slip rate since the Late Pleistocene (Ren et al., 2007). However, the investigation of the seismogenic faults of the Eryuan Earthquake in 2013 revealed that the most active faults since the Holocene are normal faults (Huang et al., 2015). The Jianchuan fault is an NNE-striking sinistral strike-slip fault (Wang et al., 1998), which has a horizontal slip rate of 3.10–6.45 mm/yr (Tang et al., 2014). In addition to the Tongdian–Weishan fault, all the other faults in the Dali fault system have a clear bending deformation at the end, which is considered to be a typical structural feature of the end of tensional–torsional fault (Wu et al., 2009, 2015).

The Dali fault system is a significant earthquake-prone area, owing to strong fault activity. From 780 A.D. to 2018 A.D., about 70 earthquakes of $M \geq 5$ were attributed to the motion along the main faults of the Dali fault system. Earthquakes, especially macroseism ($M \geq 7.0$), are generally concentrated at the four corners of the rhombic-shaped Dali block, where the faults exhibit arc bending (Figure 2). This is probably related to the concentration of stress at the end of the Dali block. Focal mechanisms and the study of historical earthquakes indicate that earthquakes in this region are mainly caused by normal faulting and the direction of principal stress is roughly N–S (Wang et al., 1997; Guo et al., 1998; Mao et al., 2003; Han et al., 2004).

At least 11 earthquakes of $M \geq 5$ were attributed to motion along the Chenghai fault zone, and two of them are of $M \geq 7$ (Table 1). The 1515 Yongsheng earthquake ($M \geq 7.5$) is the strongest historical earthquake in the Dali block (Huang et al., 2018). The coseismal surface rupture of this historical earthquake extended ~42 km and was considered to be the result of normal faulting along the Jinguan–Chenghai fault zone (Guo et al., 1998). In 1652, another macroseism occurred at the southern end of the Midu basin, which was attributed to right slipping along the Red River fault (Mao et al., 2003). However, compared with the remarkably normal faulting, evidence regarding the right-lateral slip on the Midu segment of the Red River fault is lacking (Wang et al., 1998). In addition, the shape of the meizoseismal area is short and thick ellipse, more like the normal fault type, indicating that this earthquake is more likely to be the result of normal faulting on the Chenghai fault zone. If this hypothesis is correct, then the two M ≥ 7 earthquakes can be attributed to normal faulting of the Chenghai fault zone. Focal mechanisms of medium earthquakes show that in addition to normal faulting, the Chenghai fault zone also has left-lateral motion, especially in the middle segment. However, the largest magnitude was only M 6.3, much less than those two normal faulting-type earthquakes. Seismic data show that the Chenghai fault zone has been active during the Holocene, and there have already been several M ≥ 7 earthquakes on it.

2.2 Geomorphological and Late Cenozoic sediments

Due to Late Cenozoic extensional deformation, the Dali block is characterized by a typical basin and range topography. A low-relief planation surface was recognized atop mountains at an altitude of 2400–3600 m a.s.l and was known as part of the ancient landscape in the eastern Tibetan Plateau (Cui et al., 1996; Wang et al., 1998, 2006a; Clark et al., 2004, 2006). This gradual geomorphic surface dipping to the southeast is characterized by perfectly round low-relief monadnocks with thick laterite weathering surface and occasional karst landscapes and has been dismantled by normal fault. As an ancient landscape formed before the extensional deformation of the Dali block, it constitutes a geomorphic marker for Late Cenozoic deformation along the fault system.

With the dismantling of the above planation surface, numerous extensional basins develop along the Dali fault system. A set of fluvial lacustrine sediments, named Sanying Formation

(BGMR of Yunnan Province, 1990), were deposited within the Dali block, thus recording the Late Cenozoic activity of the Dali fault system (Wang et al., 1998). The Sanying Formation consists of clay, silt with a few gravel, and peaty clay. It is similar to the Xigeda Formation, which was assumed to consist of Pliocene sediments (Wang et al., 2006b; Yao et al., 2007). It is unconformities contact with the underlying Miocene or earlier strata. According to the stratigraphic sequence and flora assemblages, the Sanying Formation is assigned to be the Late Pliocene (BGMR of Yunnan Province, 1990). The sequence exposed by the Heqing deep drilling core covers the last 2.78 Ma based on the results of AMS ^{14}C and magnetostratigraphic dating (Xiao et al., 2010). In the Jianchuan basin, the cosmogonic nuclide burial ages of the overlying Quaternary sediments indicate that the Sanying Formation is older than 2.0 Ma (Zheng et al., 2014). In addition, high-resolution magnetostratigraphic results west of the Eryuan basin indicate that the age of the Sanying Formation is from 7.6 to 1.8 Ma (Li et al., 2013, 2014).

3 The Chenghai fault zone

The Chenghai fault zone is the eastern boundary of the Dali fault system, located at the northwest end of the Red River fault (Figure 1, 2). It is considered to have experienced multiple periods of activities (Li and Jin, 1990; Fan et al., 2006; Wang et al., 1998). The activities during the pre-Cenozoic juxtapose very different lithostratigraphic units between the Dali block and Chuxiong basin. The latter obviously lacks Paleozoic strata (Figure 3). Since the Cenozoic, the fault has experienced at least two periods of activity. The earlier may start in the middle-late Paleogene (Lacassin et al., 1996; Fan et al., 2006), where older west-dipping thrust fault carried Paleozoic rocks eastward above Mesozoic and Cenozoic rocks of the Chuxiong basin (Wang et al., 1998). In addition, the older strike-slip fault dextrally displaces the Triassic strata on the west side of the Binchuan basin (Figure 3). The latest activity probably originated in the Pliocene to early Quaternary (Wang et al., 1998), where the left-lateral fault offsets rivers and streams, controlled by a series of Quaternary basins from Yongsheng to Midu. The multiple periods of activities resulted in the complex structure of the Chenghai fault zone. Early studies suggest that the Chenghai fault zone is composed of the basin controlling faults from Yongsheng to Midu and the parallel faults in Dachang–Pingchuan–Xiangyun area to the east (Li and Jin, 1990). However, the geomorphological features from Dachang to Pingchuan show that the latter has no obvious activity in the Quaternary (Figure 2). Therefore, the Chenghai fault zone discussed in this paper refers to a series of transtensional faults controlling the development of the Quaternary basins from Yongsheng to Midu area and with obvious activities since the Pliocene–Quaternary.

3.1 Fault segmentation

Here, we provide a detailed mapping of the Chenghai fault zone from the analysis of remote sensing data and field investigation. Remote sensing data include SRTM DEM (90-m resolution), Google Earth satellite image, and Google topographic map. Fieldwork is mainly conducted through large-scale investigation along the fault trace. Our mapping shows that the Chenghai fault zone trends roughly N–S and extends about 200 km from Yongsheng basin in the north to the Midu basin in the south, with complex structure and kinematic features (Figure 3).

The main characteristic is that a series of Quaternary basins with different shapes are present on the downthrow side of the fault. Evidence of an active dip slip is shown along its trace. There is also clear evidence for a component of left slip on the Chenghai fault zone. The Jinsha River intersects the middle of the fault with 5–6 km left-lateral offset. The rhombic Qina pull-apart basins north of Jinsha River are also the result of the left-slip fault. The Chenghai fault zone clearly belongs to an oblique-slip fault with both normal and left-slip components.

Along the Chenghai fault zone, five segments with a length of ~25−50 km have been identified (Figure 3) using different geometrical structures and kinematic features. At the northernmost end is the Yongsheng–Chenghai segment, and to the south, there are the Qina, Binchuan, Maolipo, the Midu segments, successively.

3.2 Kinematic characteristics of different segments

3.2.1 The Yongsheng–Chenghai segment

Fault in this segment extends ~50-km long and is mainly composed of three arc-shaped normal faults bending eastward. From west to east, there are the Jinguan–Chenghai ($F_{1–1}$), Yongsheng ($F_{1–2}$), and Muerping–Yangping faults ($F_{1–3}$), successively. Along those faults are the three levels of stepped fault basin that forms a stepped landform, indicating that those faults have significant vertical activity.

Jinguan–Chenghai fault ($F_{1–1}$): This arc-shaped, W–SW-dipping fault extends about 45 km from the northern end of the Jinguan basin in the north to the southern end of the Chenghai Lake in the south. The 1515 Yongsheng earthquake was considered to have occurred on this fault (Guo et al., 1988; Huang et al., 2018). In the north of Jinguan town, the fault strikes NW, where a series of prominent triangular facets is distributed along it, with Late Pleistocene alluvial–proluvial fan at the bottom of those facets. From Jinguan town to Pimi village, the strike of this fault gradually changes to roughly N–S. Huge, steep, 700–800-m-high fault scarps have developed along this section of the fault. At least six large ancient landslides and a deep-cutting ~300-m-deep gorge appeared on the footwall of the Jinguan–Chenghai fault (Figure 4，Figure 6a, b). South of Pumi, the fault trace is characterized by a series of subdued and linearly aligned triangular facets in Mesozoic clastic strata (Figure 5b). All these evidences show that the fault has strong normal faulting.

In addition, several secondary normal faults parallel to the Jinguan–Chenghai fault are present in the Jinguan basin (Huang et al., 2016). Tectonic geomorphologic features suggest that they may extend into Chenghai Lake. Bathymetric charts of Chenghai Lake show that the west side of the lake is deeper than the east side (Li et al. 1990) (Figure 6a), which may be related to the activity of those secondary faults.

Along the Jinguan–Chenghai fault, a cataclastic fault zone is exposed at the bottom of those triangular facets and fault scarps. The fault trace is marked by catalase, concentrated cleavage, slickensides, and fault striae (Figure 6). Near Muke fault exposed in Triassic limestone and vertically offset the stratum (Figure 6c). The main fault plane is smooth and covered with a 4–7-cm-thick fresh calcium layer. Slickenlines on those calcium layers indicate a dip-slip motion of this fault. The statistics of striation data along the Jinguan–Chenghai fault shows that the main activity of the Jinguan–Chenghai fault is dip slip, although southward along the fault, the strike-slip component gradually increases south of Pumi (Figure 4, 5).

Yongsheng fault ($F_{1\text{–}2}$): This fault extends ~30 km from Fuxing in the north to the south end of Yongsheng basin in the south and strikes N–NW. Two Quaternary basins are controlled by this fault. Among them, the Fuxing basin is smaller, and its boundary is more uneven, indicating that the activity on this fault is weaker in the north. Southward, the Yongsheng basin strikes N–S, extends ~15 km, and is bounded by triangular facets that follow a linear fault trace on its eastern side (Figures 4, 8a), indicating the obvious dip-slip activity of the Yongsheng fault.

Field investigation shows that the faults are mainly developed in Triassic clastic strata. Northeast of the Yongsheng basin, a stream is vertically offset ~17.5 m and forms a waterfall (Figure 8b). The constructional terrace ~15 m above the river is also vertically offset by the fault, showing that the fault has been active since the Late Pleistocene. Southward, three-level terraces on the footwall have also been vertically offset by persistent normal faulting since the Late Quaternary. T_3, T_2, and T_1 are about 70 m, 25 m, and 8–10 m above the river, respectively, while the vertical displacement may be about 70 m, 20 m, and 5–8 m, respectively (Figure 8d). The statistics of striation data show that the Yongsheng fault is a remarkably extensional normal fault.

Muerping–Yangping fault ($F_{1–3}$): This arc-shaped fault strikes N–NW and extends ~30 km. Two narrow Late Cenozoic fault basins, namely, the Muerping and Yangping basins, are controlled by this fault. Among them, the Muerping basin is larger and has a straighter boundary, indicating that the fault is more active toward the north. On the east side of the Muerping basin, triangular facets constitute its linear boundary, and there is no obvious drainage offset (Figure 4). There is a paleo-landslide on the footwall of the middle Muerping basin (Figure 9a), and the deposits of this landslide form a dam, dividing the basin into two parts. A fault with an attitude of 255°∠51° forms the boundary between the bedrock and landslide deposits (Figure 9b). The fault plane is smooth, and the striations on it show that the fault is dominated by normal faulting (Figure 9c).

3.2.2 The Qina segment

Southward, in the Qina segment, the Chenghai fault zone makes a ~30°sudden strike change between the Yongsheng and Chenghai segments, which strike at ~30°, and it consists of two left-stepping faults, namely, the Qina fault ($F_{2–1}$) and the Jinjiang fault ($F_{2–2}$). Between those two faults is a typical rhombic-shaped pull-apart basin (Figure 10).

Qina fault ($F_{2–1}$): This fault extends from Jajuan village to the western side of the Qina basin and is about 18-km long and strikes in NNE direction (Figure 10). North of Lishan village, the fault dips westward and expresses significant linear fault scarps (Figure 11a). These fault scarps are about 550–600-m high in Permian limestone, which clearly resulted from normal faulting along the Qina fault.

In addition, along this fault, two parallel streams have been offset left laterally at ~120 m and ~200 m, respectively (Figure 10b), indicating that the fault motion has both a dip-slip and left-lateral component. On the west side of the Qina basin, the fault dips east and is characterized by a series of linearly arranged triangular facets and fault scarps. There is a paleo-landslide (2.2-km wide) off the fault scarp (Figure 11a), which may be related to the fault activity.

At the bottom of the above paleo-landslide is a ~20-m-high fresh fault scarp in Paleozoic limestone, which left laterally offsets a small gully about 50–60 m (Figure 11b). This beheaded gully shows that the Qina fault has both normal and left-lateral slip and has been active during the Late Pleistocene to Holocene. Southward, the cataclastic fault zone exposed in the stream wall is about 15–20-m wide and is characterized by a number of subvertical faults and lenticular limestone blocks (Figure 11c). The attitude of the primary fault is about 315°∠70°, and measurements of the striations show that the fault is dominantly left lateral with normal component (Figure 11d), where the ratio of lateral to vertical slip is about 2.2:1, consistent with the ratio calculated by stream offset.

Jinjiang fault ($F_{2\text{–}2}$): This fault extends about 20 km from the east side of the Qina basin to the north end of the Binchuan basin. On the north side of the Jinsha River, the fault appears as a line of triangular facets, and a stream is left laterally offset up to 400 m along this fault (Figure 10c). The present riverbed of the Jinsha River is left laterally offset by the Jinjiang fault about 3.5 km. However, our field survey found that there is a well-sorted and well-rounded gravel layer covered by Pliocene–Pleistocene lacustrine strata around Majiawan. Using this apparent ancient riverbed as a kinematic marker, we estimate that the total left-lateral displacement along this fault is about 5–6 km since the onset of the Chenghai fault zone (Figure 10a). South of the Jinsha River, the fault can be traced by a large, steep fault scarp that extends to the eastern Binchuan basin. On the north bank of Jinsha River, a number of subvertical faults have developed in Paleozoic limestone (Figure 11e). The attitude of the main fault is 290°∠73°, and lineation on the slickensides shows that this is a strike-slip fault.

3.2.3 The Binchuan segment

This segment extends from Reshuitang in the north to Laomaying in the south and is about 50-km long and up to 35-km wide. It consists of at least five fault branches that splay out into horsetail shape structure (Figures 12). These branches include the Binchuan fault (F_{3-1}), which forms the eastern boundary of the Binchuan basin, the NE–SW striking Shangcang–Yupeng fault (F_{3-2}), which forms the western boundary of the Binchuan basin, the Pianjiao–Binju fault (F_{3-3}), the Pianjiao–Daying fault (F_{3-4}), and the Hequ fault (F_{3-5}). These faults control the complex Binchuan basin together.

Binchuan fault (F_{3-1}): This fault extends about 55 km along the eastern boundary of the Binchuan basin, forms an arcuate fault bend to the east, and is marked by a line of triangular facets exposed in Mesozoic clastic rock (Figure 12). According to the difference of height and erosion degree, the triangular facets can be divided into three levels (Figure 13a). In general, the taller triangular facets are older and more heavily eroded. Multiscale triangular facets form conspicuous evidence of the long-term, multistage activity of this fault. East of Reshuitang, the fault offsets

East of Reshuitang, the fault appears as a 600–800-m-high fault scarp. Stream along this fault is vertically offset ~200 m and forms a V-shaped hanging valley (Figure 13b). A limestone ridge left laterally offsets a stream about 1100 m (Figure 10d). The young stream formed on this basin is left laterally offset about 70 m, indicating that the fault also has a left-lateral motion component in addition to normal faulting. The cataclastic fault zone exposed on the stream wall is about 20–30-m wide, which is comprised of several high-angle faults (Figure 13c). The attitude of the master fault is 267°∠56°, and striations on it show that the fault has both left-lateral and normal motion (Figure 13d).

Southward, steep fault scarps give way to gently sloping, eroded triangular facets, with the change in lithology. Near Pianjiao, about 200-m-thick Pliocene–Pleistocene strata are exposed in west-striking gully. The dip angle is about 30° at the bottom of the sequence, which flattens out at the top, indicating that the Binchuan fault is a synsedimentary fault.

East of Binchuan, the fault strikes N–S and can be traced by a large and steep fault scarp. Under the scarp is a cataclastic fault zone, which is comprised of fragmented, lenticular limestone and a number of brittle faults. Near Zhoucheng, the fault strikes NNE, and the trace is expressed as gently sloped, weathered triangular facets. Statistical analysis of fault kinematics from measurements of the main fault striations shows that the Binchuan fault is dominated by normal faulting. The strike-slip component gradually decreases from both ends toward the middle of the fault and completely disappears east of Binchuan (Figure 12).

Shangcang–Yupeng fault ($F_{3\text{–}2}$): This NE-striking, SE-dipping fault extends about 45-km long from Reshuitang in the north to Wase in the south and forms the western boundary of the Binchuan basin. The fault trace appears as a line of triangular facets and fault valleys (Figures 12, 15a). Based on the apparent offset of drainages and other kinematic markers, the Shangcang–Yupeng fault at first seems to be right-lateral slip (Fan et al., 2006); however, our investigation reveals that the fault motion is actually left lateral. East of Reshuitang, this fault left laterally offsets the beheaded stream mentioned above about 600 m (Figure 10d). Near Shangcang, two parallel streams and the ridge between them have been left laterally offset about 1.5 km; near the middle section of the fault, a stream has been offset about 2.5 km (Figure12). In addition, the fault motion has an obvious dip-slip component since the ancient landscape on the hanging wall has been downthrown about 800 m. moreover, near Huaqiao, the fault controls a narrow faulting basin, providing evidence of dip slipping.

Field investigation showed that cataclastic rocks are common along the fault. West of Duifang, there is a fracture zone composed of several subvertical faults in Paleozoic limestone. The attitude of the main fault is 136°∠80° (Figure 14b), and measurements of striations confirm that the fault motion is dominated by left-lateral slip with a partial normal faulting.

Pianjiao–Binju fault ($F_{3–3}$): This is an N-striking, E-dipping secondary fault that extends about 50 km from just north of Pianjiao to south of Binju and terminates west of the Malipo fault (F_4). Near Pianjiao, Pliocene lacustrine sequence with an orientation of 110°∠9° exposes an E-dipping normal fault (Figure 14c). Together with the Binchuan fault, it forms a graben that has controlled the development of the Lijiao–Pianjiao, Binchuan, and Zhoucheng depositional center during the Late Cenozoic. To the south, the fault is intermittently exposed, bounding a series of mountain ranges. South of Binju, the fault bounds a nearly N-striking valley and ends west of the Maolipo fault. A stream has been left laterally offset about 1.5 km, indicating that the motion of this fault also has a partial transverse component (Figure 12).

Pianjiao–Daying fault ($F_{3–4}$): This fault extends from west of Pianjiao, south through Daying, and finally terminates north of the Wase–Binju fault. It is ~30-km long, strikes N–NW, dips E, and is composed of at least three branches. North of Lijiao, the fault is N striking and parallels the Pianjiao–Binju fault. Field investigation showed that the Pianjiao–Daying fault cuts through Pliocene strata, dropping the block on the east side of the fault (Figure 14d). Southward, the strike of this fault gradually changes to northeast, paralleling the Shangcang–Yupeng fault to the west. The trace appears as a line of triangular facets and a fault valley. East of Xiaoyindian, the attitude of the fault plane that is buried under triangular facets is 127°∠48°, and striations show that the fault motion is dominantly normal with a left-slip component.

Hequ fault ($F_{3\text{–}5}$): This W-dipping normal fault extends about 15 km from Reshuitang to Hequ. Together with the Pianjiao–Daying fault, it controls the Pliocene lacustrine horst north of the Binchuan basin (Figure 12). East of Hequ, there are several stair-stepping normal faults dipping west (Luo et al., 2015).

In summary, the N-striking faults are the largest and most active in the Binchuan basin, controlling its overall shape. The secondary NE-striking faults control the western boundary of the basin, while the NW-striking faults are the least active. Intersections between NW-striking faults crosscut by N-striking faults show that the NW-striking faults are older and recently inactive. Without the NW-striking faults, a complex graben structure (Figure 12b) is formed by the system of ~N-striking and NE-striking faults. Moreover, these faults likely converge at depth, forming a negative flower structure, which is a common behavior for transtensional fault systems.

3.2.4 The Maolipo segment

To the Maolipo segment, the Chenghai fault zone reconverged into a single left-lateral strike-slip fault with NE–SW orientation, named the Maolipo fault.

Maolipo fault (F_4): This fault extends about 25 km from Laomaying to Sujiazhuang and appears as a linear fault valley (Figure15a). Along this fault, a series of parallel drainages are left laterally offset about 1.2–1.5 km (Figure 5a), clearly indicating the active left-lateral movement of this fault. In addition, the Mesozoic granitic pluton south of Malipo has also been left laterally offset about 1.5 km (Figure 3), and it can be used as the cumulative displacement of this fault. On the northern part of the fault, four young, rapidly incising streams are left laterally offset 270–400 m (Figure 15b), indicating that the fault still has obvious left-lateral strike-slip activity since the Late Quaternary. The motion of the Maolipo fault also has an apparent dip-slip component, leading to the elevation difference of ~400 m between the planation surfaces on either side of the fault (Figure 15d).

Field survey shows that a cataclastic fault zone is exposed along this linear fault valley. At site 41, a fracture zone, consisting of numerous subvertical faults and a major fault with an orientation of 290°∠81° (Figure 15c), forms the boundary between the Devonian limestone and the Permian basalt. The fault plane is smooth and contains striations, indicating left-lateral motion with a minor dip-slip component.

3.2.5 The Midu segment

This segment extends ~30 km from Sujiazhuang in the north to Juli in the south. The Midu segment consists of the Midu fault ($F_{5\text{–}1}$) that bounds the west side of the Midu basin, the Yinjie fault ($F_{5\text{–}2}$) that forms the southeastern boundary, and a series of secondary faults within and near the basin.

Midu fault ($F_{5\text{–}1}$): This fault extends ~30 km from Sujiazhuang to Juli along the western boundary of the Midu basin (Figure 16). North of Qiaotoushao, the fault strikes northeast and appears as a ~600-m-high fault scarp in Devonian limestone. South of Qiaotoushao, the fault strike gradually turns to northwest, and the fault trace is marked by a line of triangular facets in Mesozoic clastic rock (Figure 17c). A large number of Late Pleistocene–Holocene alluvial fans are distributed linearly along the fault and extend eastward to the basin central (Figure16), indicating that the fault has been active since the Late Pleistocene. Near Guqin, the fault splays into multiple branches and controls the stepped landforms at the edge of the Midu basin and several intermountain basins on its west. These geomorphic features indicate that the Midu fault is a remarkably normal fault, and there is no geomorphic evidence of right-lateral slip.

West of Gucheng, a 100-m-wide fracture zone composed of at least four branches is exposed in Devonian limestone (Figure 17a). Those faults offset not only the limestone but also the lateritic weathering crust and deluvium on it, indicating that the fault experienced normal faulting during the Late Pleistocene–Holocene. Among them, the easternmost fault cuts through cataclastic limestone at an orientation of 158°∠72° (Figure 17b). Slickenlines on it show that this fault also has left-lateral in addition to dip-slip motion.

West of Guqin, a suite of Pliocene alluvial deposits rests unconformably on Cretaceous strata and forms a platform with an elevation of 1800–1810 m. The leading edge of the platform is vertically offset by the eastern branch of the Midu fault, forming a series of gentle triangular facets that have developed Holocene-age alluvial fans (Figure 16). Further west, a fault zone composed of three branch faults vertically offsets Cretaceous strata and Pliocene deposits that rest on it, and the attitude of the main fault is 143°∠63° (Figure 17d). On the west side of the Midu basin, there is a series of intramontane basins, the Pinganzhuang basin, the Dashuping basin, and the Dapingdi–Longshan basin, each filled with Pliocene strata. The Dashuping basin contains a sequence of lacustrine strata comprised of grayish-green mudstone, gravel-bearing sandstone, and lignite. The attitude of the bedding is about 138°∠5°; it forms a platform with an elevation of 2160–2180 m, about 350–380 m above the platform in the foothills.

Yinjie fault (F_{5-2}): This fault extends about 18 km from Midu to Juli along the eastern boundary of the Midu basin. This SW-dipping fault is marked by a line of scarps and triangular facets. Slickensides, dislocation breccia, and hot springs are common along this fault. East of

Qingshiwan, a ~30-m-wide cataclastic fault zone is exposed in Permian limestone, and the attitude of the main fault is 230°∠62°.

3.3 Kinematic characteristics of the Chenghai fault zone

The Chenghai fault zone is generally considered to be a left-slipping fault rather than a normal fault (Wang et.al., 1998; Fan et.al., 2006). However, evidences from the detailed mapping of the Chenghai fault zone show that it is an oblique-slip fault with both normal and sinistral strike-slip components, and normal faulting is more significant. The evidences are as follows. First, normal faults control the development of all fault basins except the Qina basin. Second, geomorphological and geological evidence, particularly the statistics result of striations, show that, except for the Qina and Maolipo segments, the whole Chenghai fault zone is dominated by normal faulting. Third, the largest left-lateral displacement, a 5–6-km offset that occurs in the Qina segment, is smaller than the width of the extensional fault basin. Finally, seismic data since 780 A.D. shows that $M \geq 5.0$ earthquakes (including two $M \geq 7$ earthquakes) along the Chenghai fault zone mostly occur along those normal fault segments (Figure 2).

3.4 Million-year-scale rates of the Chenghai fault zone

As mentioned above, the Chenghai fault zone is mainly exposed in bedrock strata, it is difficult to determine the short time scale activity rates of this fault zone. Therefore, in this paper, only the rate of fault on the million-year-scale will be discussed. However, the accurately starting time of the transtensional motion along the Chenghai fault zone is not clear. Most previous studies suggest that transtensional motion of the Chenghai fault zone has begun since the Quaternary (Li et al., 1990; Fan et al., 2006). Wang et al. (1998) believed that the Dali fault system faulting began at ~4 Ma, similar to the latest period of movement on the Red River fault system. Based on the age of sediments deposited in extensional basins, the cooling history of the Diancang Mountain and the starting time of right–lateral motion along the Red River fault, we believe that the motion along the Chenghai fault zone probably started in Early Pliocene.

As a sign of the beginning of transtensional deformation of the Dali fault system, there have different understanding about the formation age of the Sanying Formation (BGMR of Yunnan Province, 1990; Xiao et al., 2010; Li et al., 2013, 2014; Zheng et al., 2014) (Figure 18). In Yongsheng and Midu basins the outcropping of the Sanying formation is very limited, only a few tens of meters thick. It mainly consists of interbedded gravel, sand and silt, in Midu basin there is a small amount of peaty clay exposed in the lower part of this stratum (Figure 18). In Binchuan basin, the Late Cenozoic sediments are about 200m thick, and can be divided into two distinct groups. The bottom is 30–40m thick gravel layer similar to the outcropping in Yongsheng and Midu basins belong to the Sanying Formation. The upper part is a group of interbedded clays, silt and fine–grained sands may belong to the Xigeda Formation. And the former is disconformity onlapped by the latter one (Figure 18). The age of Xigeda Formation exposed in Panzhihua (cosmogonic nuclide burial age1.34–1.58 Ma) (Kong et al., 2009).

The variability in the ages of the Sanying formation may be related to the different outcropping between various basins. For example, in Eryuan basin the Sanying formation is about 1000 meters thick, and can be divided into four facies associations (FA) (Li et al., 2013, 2014). Compared to the Sanying Formation in other basins (Figure 18), we suggest that only FA2 and FA3 belong to the Sanying Formation. The stratigraphic sequence of FA1 show that it is more consistent with the definition of the middle Miocene Shuanghe Formation (BGMR of Yunnan Province, 1990), and FA4 may be belongs to Quaternary gravel strata. Therefore, we suggest that the upper age limit of the Sanying Formation in the Dali block is about 6 Ma, and can be used as the onset activity time of the Dali fault system.

Cooling history of the Diancang Mountain from a K–feldspar $^{40}Ar/^{39}Ar$ age spectrum records a rapid cooling event at about 4.7 ± 0.1 Ma (Chen and Harrison, 1992; Leloup, et, al., 1993). This cooling event may represent exhumation which was structurally related to extensional deformation of the Dali fault system and the Chenghai fault zone. Third, previous studies on the main faults between the Red River fault and the Sagaing fault show that the Cenozoic tectonic inversion occurred in this region between 5–20 Ma and near the Red River fault stress field and slip–sense inversion was happened around 5 Ma (Lacassin et al., 1998). The Red River fault itself has reversed to right–lateral motion about 5 Ma (Tapponnier et al., 1990；Harrison et al., 1992; Replumaz et al., 2001).

In summary, based on those evidences it can conclude that the transtensional activity of Chenghai fault zone started in the Early Pliocene about 5–6 Ma. Then the average slip rate of the Chenghai fault zone can be calculated since 5–6 Ma (Table 2).

Without considering the weathering and denudation, the cumulative vertical displacement of the Chenghai fault zone is equal to the height difference between the basin surface and the paleogeomorphic surface plus the thickness of the late Cenozoic sediments in the basin. Among them, the height difference is measured based on SRTM DEM (90-m resolution), and the sediment thickness data mainly comes from the regional geology of Yunnan (BGMR of Yunnan Province, 1990). In addition, the accumulated horizontal displacement is measured according to the offset of water system, geological and geomorphic bodies, such as the left laterally offset of the Jinsha River.

Based on the above data, the million-year-scale rates of the Chenghai fault zone can be estimated, see Table 2 for details. Along Chenghai fault zone the most intense normal faulting occurred on the Yongsheng–Jinguan segment with a dip–slip rate of 0.37–0.57 mm/yr, and the most intense left–slipping occurred in the Qina segment with a strike–slip rate of 0.83–1.20 mm/yr.

4 Discussion

The geometric and kinematic geological characteristics, as well as the seismic activity along the Chenghai fault zone, indicate that the Dali block has a clockwise rotational motion relative to its surrounding area. Firstly, the Chenghai fault zone is curved at both ends, forming a rough Z-shaped pattern. In fact, most of the faults in the four corners of the Dali fault system exhibit this pattern through the strike. The evaluation and analysis of the Piedmont fault of the Haba–Yulong Snow Mountain (HYPF) show that the arc bending at the end of a fault is a typical structure formed in response to the clockwise torsional stress (Wu et al., 2009). Secondly, the slip rate of the Chenghai fault zone increases toward the end, especially on the Yongsheng–Chenghai segment. In fact, the HYPF and the Eastern Piedmont fault of Diancang Shan (located at the corners of the Dali block) are the most active faults in this region: the average slip rate on the HYPF is around 0.3–1.4 mm/yr since the Late Quaternary (Wu et al., 2009). Thirdly, seismicity data indicates that strong earthquakes are generally concentrated with lethal intensity at the four corners of the diamond-shaped Dali block, where the faults exhibit arc bending. Four $M \geq 7.0$ earthquakes recorded in this area have occurred in each corner of the Dali block. The concentration of earthquakes and fault motion at the ends of the Dali block suggest that higher stress with optimum intensity is concentrated at the end of the Dali fault system arc bending zone. Like the arc bending at the end of the fault, these features formed in response to the clockwise rotation of the Dali block. Besides, the paleomagnetic study of the Sanying Formation in the Eryuan basin indicates that there is a 4.4 ± 2.5° clockwise rotation in the Dali area since the Late Miocene (Li et al., 2013). The paleogeomagnetic study of the Eocene–Miocene strata in the Jianchuan area also suggests that since the Miocene, there has been a 15°–20° clockwise rotational deformation relative to East Asia (Tong et al., 2015).

As a remarkable Late Cenozoic extensional deformation zone, the Dali fault system remains the focus of attention. Several models have been suggested to explain the formation mechanism of this area. An earlier study of the Red River fault proposed that the extensional deformation in the Dali fault system resulted from the end extension of the Red River fault (Allen et al., 1984). Some scholars believe that the Dali fault system resulted from a pull-apart between the Zhongdian fault and the Red River fault (Zhang et al., 2015). Wang et al. (1998) attributed the extension of the Dali system to the clockwise rotational motion of micro-fault blocks along with the end extension of concomitant strike-slip faults. However, the suggested models cannot explain the clockwise rotation of the Dali fault system and the Chenghai fault zone.

Take a broad view to the SEMTP, deformation in and around this region is featured by a set of large-scale strike-slip faults that developed and evolved around the eastern Himalayan syntaxis (EHS) (e.g., Tapponnier et al., 1986; Allen et al., 1991; Leloup et al., 1995; Wang and Burchfiel, 1997; Wang et al., 1998) (Figure 19). The left-lateral Xianshuihe–Xiaojiang fault system (XXF) was initiated within the range of 13–5 Ma (Roger et al., 1995; Zhu et al., 2008; Wang et al., 2009), with a 60–80-km displacement (Allen et al. 1991; Wang et al. 1998) and short-term slip rates of up to 7–11 mm/yr (Shen et al., 2005). The Red River fault (RRF) was a ductile left-lateral shear zone from 35 to 17 Ma (Tapponnier et al., 1990; Leloup et al., 1993) and a brittle right-lateral fault from the Pliocene to the present (Leloup et al., 1993; Lacassin et al., 1998). Since the Pliocene, the RRF functions as the western boundary of the Chuandian Fragment and accommodates its southeastward extrusion together with the XXF (Tapponnier and Molnar, 1976; Tapponnier et al., 2001). The Dien Bien Phu fault (DBPF) appears southwest of the RRF, sharing the spatial alignment with the XXF, while the tectonic shear on this fault is considered to transmit across the Red River fault and is regarded to be taken up by the XXF (Wang et al. 1998; Lai et al., 2012). Sinistral displacement along the DBPF could be averaged up to 12.5 km, and the Pliocene to present average slip rate is about 2.5 mm/yr (Lai et al., 2012). The Nantinghe and the Wanding are two significant left-lateral faults located approximately parallel to the DBPF. Since the Pliocene, the slip rate of both faults could be averaged up to 1.6 mm/yr and 1.9 mm/yr, respectively (Lacassin et.al., 1998). The left-lateral Litang fault is considered to have been initiated between 5 and 7 Ma, while its average slip rate is evaluated to be about 0.9–3 mm/yr (Shen et al., 2005; Zhang et al., 2015; Chevalier et al., 2016). However, to date, the slip rate of the Zhongdian fault is still a matter of debate, and it remains unclear whether the fault is left lateral or right lateral (Wang et al., 1998; Chang et al., 2013).

Among the mentioned faults, the XXF and the DBPF form a clear arcuate fault system, called the Xianshuihe–Xiaojiang–Dien Bien Phu fault system and define the eastern boundary of the SEMTP, with a clockwise rotational motion around the EHS (Wang et al., 1998). The Litang fault constitutes a smaller arcuate fault system jointly with the Dali fault system and the Nantinghe and the Wanding faults, called the Litang–Dali–Ruili fault system (Wu et al., 2015; Shi et al., 2018). These two arcuate fault systems are approximately located at the low-velocity high-electrical conductivity zone, where the crustal channel is considered to flow (Bai et al., 2010; Bao et al., 2015). The Litang–Dali–Ruili fault system extends to about 1,400 km, running approximately parallel to the Xianshuihe–Xiaojiang–DBPF system, dividing the SEMTP into two parts, namely, “the inner arcuate belt” and “the outer arcuate belt” (Wu et al., 2015). The Dali fault system, which is located at the intersection of the RRF and the Litang–Dali–Ruili fault system, is a significant extensional deformation zone, comprising of a series of active faults, including the Chenghai fault zone.

As described, with the weakening of the activity of the RRF and played a relatively weaker role as the southwest boundary of the Chuandian Fragment (Wang et al., 1998; Schoenbohm et.al, 2004, 2006). On the SEMTP, the crustal material rotates clockwise around the EHS (Wang et al., 1998; Kirby et al., 2002; Zhang et al., 2004; Shen et.al. 2005). However, crustal matter between the Yushu–Xianshuihe–Xiaojiang–DBPF and the Sagaing fault shows no rotatory signs as a rigid body; instead, its interior is in a highly deformed state (Wang et al., 1998). Drainage offsets and GPS data indicate that the average left-slip rate of the Litang–Dali–Ruili fault belt could be as high as 1–4 mm/yr during the Quaternary (Lacassin R et.al., 1998; Xu et.al., 2005; Shen et.al., 2005). Data from the left-lateral slip indicates that the angular velocity of the inner arcuate belt (clockwise rotation around the eastern syntaxis) is faster than the outer arcuate belt. In the Dali area, the difference of angular velocity is compensated by the clockwise rotation of the Dali block (Figure 19b). This leads to the bending deformation at the end of the N-trending faults, eventually forming the Z-shaped Dali fault system and the Chenghai fault zone (Figure 19c).

5 Conclusions

(1) The Chenghai fault zone strikes ~N–S, extends up to 200 km from Jinguan to the south end of the Midu basin, and curves at both ends, forming a Z-shaped structure. It is an oblique-slip fault with both normal and sinistral strike-slip components, in which the normal component is more significant.

(2) The transtensional activity along the Chenghai fault zone may have started in the Early Pliocene about 5–6 Ma. To date, the most intense normal faulting occurred on the Yongsheng–Jinguan segment with a dip-slip rate of 0.37–0.57 mm/yr, while the most intense left slipping to date occurred in the Qina segment with a strike-slip rate of 0.83–1.20 mm/yr.

(3) The difference of angular velocity between the inner arcuate belt and the outer arcuate belt leads to the clockwise rotation of the Dali block and the formation of the Z-shaped Dali fault system and the Chenghai fault zone.

Acknowledgments, Samples, and Data

- There is no real or perceived financial conflicts of interests for any author.
- There are no other affiliations for any author that may be perceived as having a conflict of interest with respect to the results of this paper.
- For theoretical papers, or most review papers: Data were not used, nor created for this research.
- This work was supported by National Natural Science Foundation of China (41571013, U2002211), China Geological Survey Project (12120114002101 and DD20160268).
- We thank Shi Xuhua for helpful discussions and suggestions; Zhang Duo, Liu Jie and Luo Ruijie for field assistance.

References

Allen, C. R., Gillespie, A. R., Han, Y., Sieh, K. E., Zhang, B. C. and Zhu, C. N. (1984), Red River and associated faults, Yun nan Province, China: Quaternary geology, slip rates, and seismic hazard. *Geological Society of America Bulletin*, 95(6), 686–700.

Allen, C. R., Luo, Z. L., Qian, H., Wen, X. Z., Zhou, H. W. and Huang, W. S. (1991), Field study of a highly active fault zone: The Xianshuihe fault of southwestern China. *Geological Society of America Bulletin*, 103(9), 1178–1199.

Anne, S., Manuel, P., (2005) Cenozoic deformation in western Yunnan (China-Myanmar border). *Journal of Asian Earth Sciences*, 24(4):495-515.

Bai, D. H., Unsworth, M. J., Meju, M. A., Ma, X. B., Teng, J. W., Kong, X. R., Sun, Y., Sun, J., Jiang, C. S. and Zhao, C. P. (2010), Crustal deformation of the eastern Tibetan Plateau revealed by magnetotelluric imaging. *Nature Geoscience*, 3(5), 358–362.

Bao, X., Sun, X., Xu, M., Eaton, D. W., Song, X., Wang, L., et al. (2015). Two crustal low–velocity channels beneath SE Tibet revealed by joint inversion of Rayleigh wave dispersion and receiver functions. *Earth and Planetary Science Letters*, 415, 16–24.

Bureau of Geology and Mineral Resources (BGMR) of Yunnan Province, (1990), Regional Geology of Yunnan Province: Beijing, Geological Publishing House, 728 pp (in Chinese).

Chang, Z. F., Zhang, Y. F., Li, J. L. and Zang, Y. (2014), The geological and geomorphic characteristic of Late Quaternary activity of the Deqin–Zhongdian–Daju fault. *Journal of Seismological Research*, 37(1): 46–52.

Chen Z., Burchfiel B. C., Liu Y., King R. W., Royden L. H., Tang W., Wang E., Zhao J., Zhang X., (2000), Global Positioning System measurements from eastern Tibet and their implications for India/Eurasia intercontinental deformation. *Journal of Geophysical Research Solid Earth*, 105(B7): 16215-16227.

Chen, W. J. and Harrison, T. M. (1992), Thermochronology of the ailoshan–red river shear zone–a case study of multiple diffusion domain model. *Seismology and Geology*, 14(2), 121–128. (in Chinese with English abstract)

Chevalier, M. L., Leloup, P. H., Replumaz, A., Pan, J. W., Liu, D. L., Li, H. B., Gourbet, L., Métois, M. (2016), Tectonic–geomorphology of the Litang fault system, SE Tibetan Plateau, and implication for regional seismic hazard. *Tectonophysics*, 682: 278–292.

Clark M. K., Royden L. H., (2000), Topographic ooze: Building the eastern margin of Tibet by lower crustal flow. Geology, 28(8): 703-706.

Clark, M. K., Royden, L. H., Whipple, K. X., Burchfiel, B. C., Zhang, X. and Tang, W. (2006), Use of a regional, relict landscape to measure vertical deformation of the eastern Tibetan Plateau. *Journal of Geophysical Research Earth Surface*, 111(F3), 1–23.

Clark, M. K., Schoenbohm, L. M., Royden, L. H., Whipple, K. X., Burchfiel, B. C., Zhang, X., Tang, W., Wang, E. and Chen, L. (2004), Surface uplift, tectonics, and erosion of eastern Tibet from large–scale drainage patterns. *Tectonics*, 23(1), TC1006.

Copley A., (2008), Kinematics and dynamics of the southeastern margin of the Tibetan Plateau. Geophysical Journal of the Royal Astronomical Society, 174(3): 1081-1100.

Cui, Z. J., Gao, Q. Z., Liu, G. N., Pan, B. T. and Chen, H. L. (1996), Planation surface, paleokarst and uplift of the Tibet Plateau. *Science in Chinese Ser. D Earth Science*, 26(4), 378–384 (in Chinese).

Dewey J. F., (1988), The Tectonic Evolution of the Tibetan Plateau. Philosophical Transactions of the Royal Society of London a Mathematical Physical & Engineering Sciences, 327(1594): 379-413.

England P., Molnar P. (1990), Right–lateral shear and rotation as the explanation for strike–slip faulting in eastern Tibet. *Nature*, 344(6262):140–142.

England, P. and Houseman, G. (1989), Extension during continental convergence, with application to the Tibetan Plateau. *Journal of Geophysical Research: Solid Earth*, 94(B12), 17561–17579.

Fan, C., Wang, G., Wang, S. F. and Wang, E. (2006), Structural Interpretation of extensional Deformation along the Dali Fault System, Southeastern Margin of the Tibetan Plateau. *International Geology Review*, 48(4), 287–310.

Guo, S. M., Xiang, H. F., Zhang, J., Hu, R. Q. and Zhang, G. W. (1988), Discussion on the deformation band and magnitude of the 1515 Yongsheng earthquake in Yunnan province. *Journal of Seismological Research*, 11(2), 153–162 (in Chinese with English abstract).

Han, Z. J., Guo, S. M., Xiang, H. F., Zhang, J. S. and Ran, Y. K. (2004), Seismotectonic environment of occurring the february (1996), Lijiang M7.0 earthquake, Yunnan province. *Acta Seismologica Sinica*, 26(4), 410–418 (in Chinese with English abstract).

Harrison, T. M., Chen, W. J., Leloup, P. H., Ryerson, F. J. and Tapponnier, P. (1992), An Early Miocene Transition in deformation regime within the Red River Fault Zone, Yunnan, and its significance for Indo–Asian tectonics. *Journal of Geophysical Research: Solid Earth*, 97(B5), 7159–7182.

Holt W. E., Ni J. F., Wallace T. C., Haines A. J., (1991), The active tectonics of the eastern Himalayan syntaxis and surrounding regions. Journal of Geophysical Research Solid Earth, 96(B9):14595-14632.

Houseman, G. and England, P. (1993), Crustal thickening versus lateral expulsion in the Indian–Asian continental collision. *Journal of Geophysical Research: Solid Earth*, 98(B7), 12233–12249.

Huang X. L., Wu Z. H., Jiang Y., Tian T. T., Liu Y. H., (2015), Seismic intensity distribution and seismogenic structure analysis of the Ms5.5 earthquake in Yunnan Dali Eryuan on march 3, 2013. Geological Bulletin of China, 34(1):135-145.

Huang, X. L., Wu, Z. H. and Wu, K. G. (2018). Surface rupture of the 1515 Yongsheng earthquake in northwest Yunnan, and its Seismogeological implications. *Acta Geologica Sinica (English Edition)*, 92(4): 1324–1333.

Huang, X. L., Wu, Z. H., Wu, K. G. and Zhou, C. J. (2016), The main active faults and tectonic system in Yongsheng area, northwestern Yunnan. *Journal of Geomechanics*, 22(3): 531–547 (in Chinese with English abstract).

Kirby, E., Reiners, P. W., Krol, M. A., Whipple, K. X., Hodges, K. V., Farley, K. A., Tang, W. Q. and Chen, Z. L. (2002), Late Cenozoic evolution of the eastern margin of the Tibetan Plateau: Inferences from $^{40}Ar/^{39}Ar$ and (U–Th)/He Thermochronology. *Tectonics*, 21(1), 1–19.

Kong, P., Granger, D. E., Wu, F. Y., Caffee, M. W., Wang, Y. J., Zhao, X. T., Zheng, Y. (2009), Cosmogenic nuclide burial ages and provenance of the Xigeda paleo–lake: Implications for evolution of the Middle Yangtze River. *Earth and Planetary Science Letters*, 278(1–2): 131–141.

Lacassin, R., Replumaz, A. and Hervé Leloup, P. (1998), Hairpin river loops and slip–sense inversion on Southeast Asian strike–slip faults. *Geology*, 26(8), 703–706.

Lai, K. Y. and Chena, Y. G. (2012), Pliocene–to–present morphotectonics of the Dien Bien Phu fault in northwest Vietnam. *Geomorphology*, 173–174(9), 52–68.

Leloup, P. H., Harrison, T. M., Ryerson, F. J., Chen, W. J., Qi, L., Tapponnier, P. and Lacassin, R. (1993), Structural, petrological and thermal evolution of a Tertiary ductile strike–slip shear zone, Diancang Shan, Yunnan. *Journal of Geophysical Research: Solid Earth*, 98(B4), 6715–6743.

Leloup, P. H., Lacassin, R., Tapponnier, P., Schärer, U., Zhong, D. L., Liu, X. H., Zhang, L. S., Ji, S. C. and Trinh, P. T. (1995), The Ailao Shan–Red River shear zone (Yunnan, China), Tertiary transform boundary of Indochina. *Tectonophysics*, 251, 3–84.

Li, G. R. and Jin, D. S. (1990), Neoid activity on the Chenghai fracture. *Yunnan Geology*, 9(1), 1–24 (in Chinese with English abstract).

Li, S. H., Deng, C. L., Paterson, G. A., Yao, H. T., Huang, S., Liu, C. Y., He, H. Y., Pan, Y. X. and Zhu, R. X. (2014), Tectonic and sedimentary evolution of the late Miocene–Pleistocene Dali Basin in the southeast margin of the Tibetan Plateau: Evidences from anisotropy of magnetic susceptibility and rock magnetic data. *Tectonophysics*, 629, 362–377.

Li, S. H., Deng, C. L., Yao, H. T., Huang, S., Liu, C. Y., He, H. Y., Pan, Y. X. and Zhu, R. X. (2013), Magnetostratigraphy of the Dali Basin in Yunnan and implications for late Neogene rotation of the southeast margin of the Tibetan Plateau. *Journal of Geophysical Research: Solid Earth*, 118(3), 791–807.

Luo, R. J., Wu, Z. H., Huang, X. L., Huang, X. J., Zhou, C. J. and Tian, T. T. (2015), The main active faults and the active tectonic system of Binchuan area, northwestern Yunnan. *Geological Bulletin of China*, 34(1), 155–170 (in Chinese with English abstract).

Mao, Y. P., Han, X. M., Gu, Y. S., He, W. and Luo, R. L. (2003), Study on strong earthquakes(M⩾6) in Yunnan area, (Kunming, China, Yunnan Science and Technology Press) (in Chinese).

Molnar P, Tapponnier P. 1975, Cenozoic Tectonics of Asia: Effects of a Continental Collision. Science, 4201(189): 419-426.

Molnar P., Lyoncaent H., 1989, Fault plane solutions of earthquakes and active tectonics of the Tibetan Plateau and its margins. Geophysical Journal International, 99(1): 123-154.

Ren, J. J., Zhang, S. M., Hou, Z. H. and Liu, X. D. (2007), Study of late Quaternaryslip rate in the mid–segment of the Tongdian–Weishan fault. *Seismology and Geology*, 29(4): 756–764 (in Chinese with English abstract).

Replumaz, A., Lacassin, R., Tapponnier, P. and Leloup, P. H. (2001), Large river offsets and Plio–Quaternary dextral slip rate on the Red River fault (Yunnan, China). *Journal of Geophysical Research: Solid Earth*, 106(B1), 819–836.

Roger, F., Calassou, S., Lancelot, J., Malavieille, J., Mattauer, M., Xu, Z., Hao, Z., Hou, L. (1995), Miocene emplacement and deformation of the Konga Shan granite (Xianshui He fault zone, west Sichuan, China): Geodynamic implications. *Earth and Planetary Science Letters*, 130(1–4): 201–216.

Royden, L. H., Burchfiel, B. C., King, R. W., Wang, E., Chen, Z. L., Shen, F. and Liu, Y. P. (1997), Surface deformation and lower crustal flow in eastern Tibet. *Science*, 276, 788–790.

Schoenbohm, L. M., Burchfiel, B. C., Chen, L. Z. and Yin, J. Y. (2006), Miocene to present activity along the Red River fault, China, in the context of continental extrusion, upper–crustal rotation, and lower–crustal flow. *Geological Society of America Bulletin*, 118(5), 672–688.

Schoenbohm, L. M., Whipple, K. X., Burchfiel, B. C. and Chen, L. (2004), Geomorphic constraints on surface uplift, exhumation, and plateau growth in the Red River region, Yunnan Province, China. *Geological Society of America Bulletin*, 116(7), 895–909.

Shen, Z. K., Lü, J. N., Wang, M. and Bürgmann, R. (2005), Contemporary crustal deformation around the southeast borderland of the Tibetan Plateau. *Journal of Geophysical Research: Solid Earth*, 110(B11), 1–17.

Shi, X., Wang, Y., Sieh, K., Weldon, R., Feng, L., Chan, C. H., Jing, L. Z. (2018), Fault slip and GPS velocities across the Shan Plateau define a curved southwestward crustal motion around the eastern Himalayan syntaxis. *Journal of Geophysical Research: Solid Earth*, 123: 2502–2518.

Socquet, A., and Pubellier, M. (2005), Cenozoic to active deformation in Western Yunnan (Myanmar China border). *Journal of Asian Earth Sciences*, 24 (2005) 495–515.

Tang, Y. and Liu, J. L. (2010), Morphotectonics of western Sichuan–Yunnan since Pliocene: The development of basins along fault zones and constraints on far–field intracontinental tectonic process. *Acta Petrologica Sinica*, 26(6):1925–1937 (in Chinese with English abstract).

Tang, Y., Hu, C., Tian, Q. J., Yang, P. X., (2014), A preliminary study of paleo-earthquakes in the Jianchuan section of Longpan-Qiaohou fault zone, Yunnan province. *Earthquake*, 34 (3), 117-124 (in Chinese with English abstract).

Tapponnier, P., and Molnar, P. (1976), Slip–line field theory and large–scale continental tectonics. *Nature*, 264(5584), 319–324.

Tapponnier, P., Lacassin, R., Leloup, P. H., Schärer, U., Zhong, D. L., Wu, H. W., Liu, X. H., Ji, S. C., Zhang, L. S. and Zhong, J. Y. (1990), The Ailao Shan–Red River metamorphic belt: Tertiary left–lateral shear between Indochina and South China. *Nature*, 343(6257), 431–437.

Tapponnier, P., Peltzer, G. and Armijo, R. (1986), On the mechanics of the collision between India and Asia. *Geological Society of London Special Publications*, 19(1), 113–157.

Tapponnier, P., Peltzer, G., Dain, A. Y. L., Armijo, R. and Cobbold, P. (1982), Propagating extrusion tectonics in Asia: New insights from simple experiments with plasticine. *Geology*, 10(10), 611–616.

Tapponnier, P., Xu, Z. Q., Roger, F., Meyer, B., Arnaud, N., Wittlinger, G. and Yang, J. S. (2001), Oblique stepwise rise and growth of the Tibet plateau. *Science*, 294(5547), 1671–1677.

Taylor M., Yin A., (2009), Active structures of the Himalayan-Tibetan orogen and their relationships to earthquake distribution, contemporary strain field, and Cenozoic volcanism. Geosphere, 5(3):199-214.

Tong, Y. B., Yang, Z. Y., Wang, H., Gao, L., An, C. Z., Zhang, X. D. and Xu, Y. C. (2015), The Cenozoic rotational extrusion of the Chuan Dian Fragment: New paleomagnetic results from paleogene red–beds on the southeastern edge of the Tibetan plateau. *Tectonophysics*, 658(2015), 46–60.

Wang, E., and Burchfiel, B. C. (1997), Interpretation of Cenozoic tectonics in the Right–Lateral accommodation zone between the Ailao shan shear zone and the eastern Himalayan syntaxis. *International Geology Review*, 39(3), 191–219.

Wang, E., Burchfiel, B. C., Royden, L. H., Chen, L. Z., Chen, J. S., Li, W. X. and Chen, Z. L. (1998), Late cenozoic Xianshuihe–Xiaojiang and Red River fault systems of southwestern Sichuan and central Yunnan, China. *Special Paper of the Geological Society of America*, 327, 1–108.

Wang, E., Fan, C., Wang, G., Shi, X. H., Chen, Z. L. and Chen, Z. L. (2006a), Deformational and geomorphic processes in the formation of the Ailao shan–Diancang range, west Yunnan. *Quaternary Sciences*, 26(2), 220–227.

Wang, S. B., Zhao, Z. Z., Qiao, Y. S. and Jiang F. C. (2006b), Age and paleo environment of Xigeda Formation in Luding, Sichuan. *Quaternary sciences*, 26(02): 257–264 (in Chinese with English abstract).

Wang, S. F., Fang, X. M., Zheng, D. W. and Wang, E. (2009), Initiation of slip along the Xianshuihe fault zone, eastern Tibet, constrained by K/Ar and fission–track ages. *International Geology Review*, 51(12), 1121–1131.

Wu, Z. H., Long, C. X., Fan, T. Y., Zhou, C. J., Feng, H., Yang, Z. Y. and Tong, Y. B. (2015), The arc rotational–shear active tectonic system on the southeastern margin of Tibetan Plateau and its dynamic characteristics and mechanism. *Geological Bulletin of China*, 34(1), 1–31 (in Chinese with English abstract).

Wu, Z. H., Zhang, Y. S., Hu, D. G., Zhao, X. T. and Ye, P. S. (2009), Late Quaternary normal faulting and its kinematic mechanism of eastern piedmont fault of the Haba–Yulong Snow Mountains in northwestern Yunnan, China. *Science in Chinese Ser. D Earth Science*, 52(10), 1470–1484.

Xiao, X. Y., Shen, J., Wang, S. M., Xiao, H. F. and Tong, G. B. (2010), The variation of the southwest monsoon from the high resolution pollen record in Heqing Basin, Yunnan Province, China for the last 2.78 Ma. *Palaeogeography Palaeoclimatology Palaeoecology*, 287(4), 45–57.

Xu, X. W., Wen, X. Z., Yu, G. H., Zheng, R. Z., Luo, H. Y. and Zheng, B. (2005), Average slip rate, earthquake rupturing segmentation and recurrence behavior on the Litang fault zone, western Sichuan Province, China. *Science in Chinese Ser. D Earth Science*, 48(8), 1183–1196 (in Chinese with English abstract).

Yao, H. T., Zhao, Z. Z., Qiao, Y. S., Li, C. Z., Wang, S. B., Wang, Y., Chen, Y. S. and Jiang, F. C. (2007) Magnetostratigraphic dating of the Xigeda formation in Mianning, Sichuan and its significance. *Quaternary Sciences*, 27(1), 74–84 (in Chinese with English abstract).

Zhang Yuan-Ze, A. Replumaz, Guo-Can Wang, P.-H. Leloup, C. Gautheron, M. Bernet, P. van der Beek, J.-L. Paquette, An Wang, Ke-Xin Zhang, M.-L. Chevalier, Hai-bing Li (2015), Timing and rate of exhumation along the Litang fault system, South East Tibet, Tectonics, 34, 934-950.

Zhang, P. Z., Shen, Z. K., Wang, M., Gan, W. J., Bürgmann, R., Molnar, P., Wang, Q., Niu, Z. J., Sun, J. Z., Wu, J. C. and Abbate, E. (2004), Continuous deformation of the Tibetan Plateau from global positioning system data. *Geology*, 32(9), 809–812.

Zheng, Y., Jia, J., Nie, X. K. and Kong, P. (2014), Cosmogenic nuclide burial age of the Sanying Formation and its implications. *Science in Chinese Ser. D Earth Scienc*e, 57(6), 1141–1149.

Zhu, R. X., Potts, R., Pan, Y. X., Lü, L. Q., Yao, H. T., Deng, C. L. and Qin, H. F. (2008), Paleomagnetism of the Yuanmou Basin near the southeastern margin of the Tibetan Plateau

823 and its constraints on late Neogene sedimentation and tectonic rotation. *Earth and Planetary*
824 *Science Letters*, 272(1–2), 97–104.

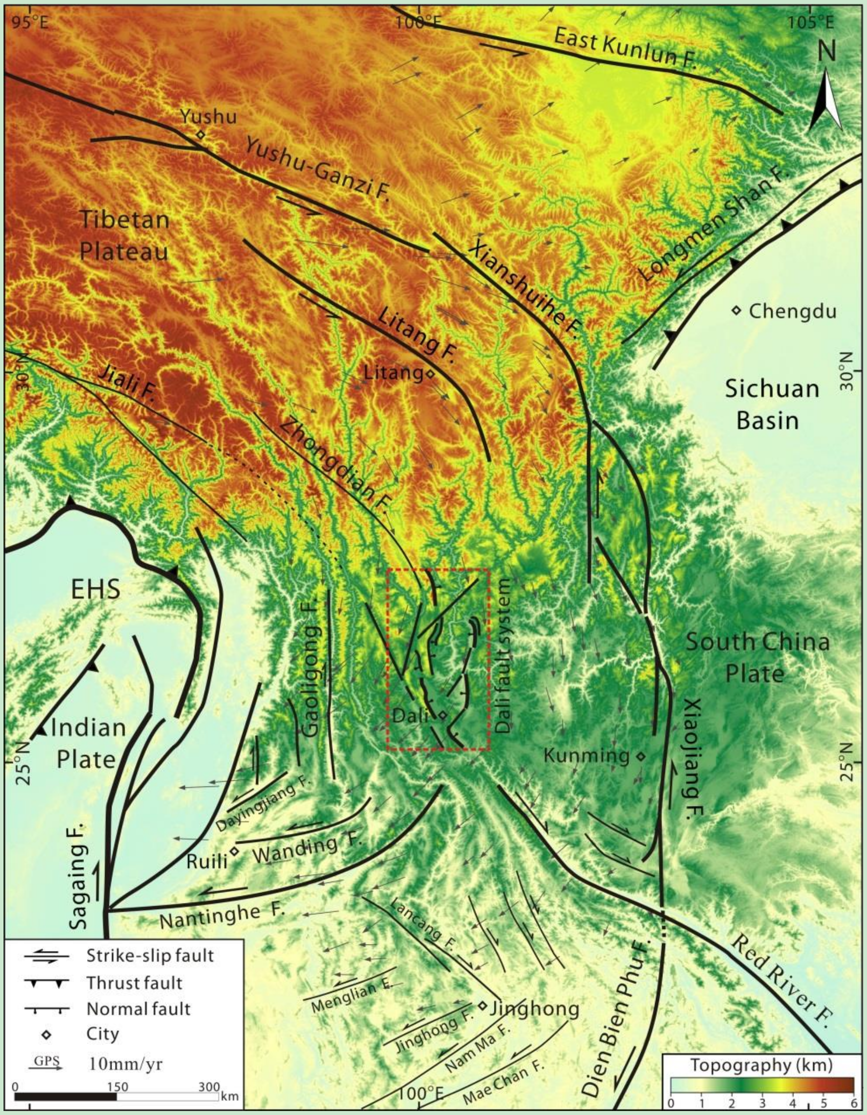

Figure 1. Major active faults within the southeastern margin of the Tibetan Plateau and its adjacent regions on digital elevation model image. Black lines represent faults (Wang et al., 1998; Tapponnier et al., 2001; Wu et al., 2015; Shi et al., 2018). Vector arrows indicate motions of the crust relative to the south China block (Shen et al., 2005). Red rectangle delineates the research area of this paper.

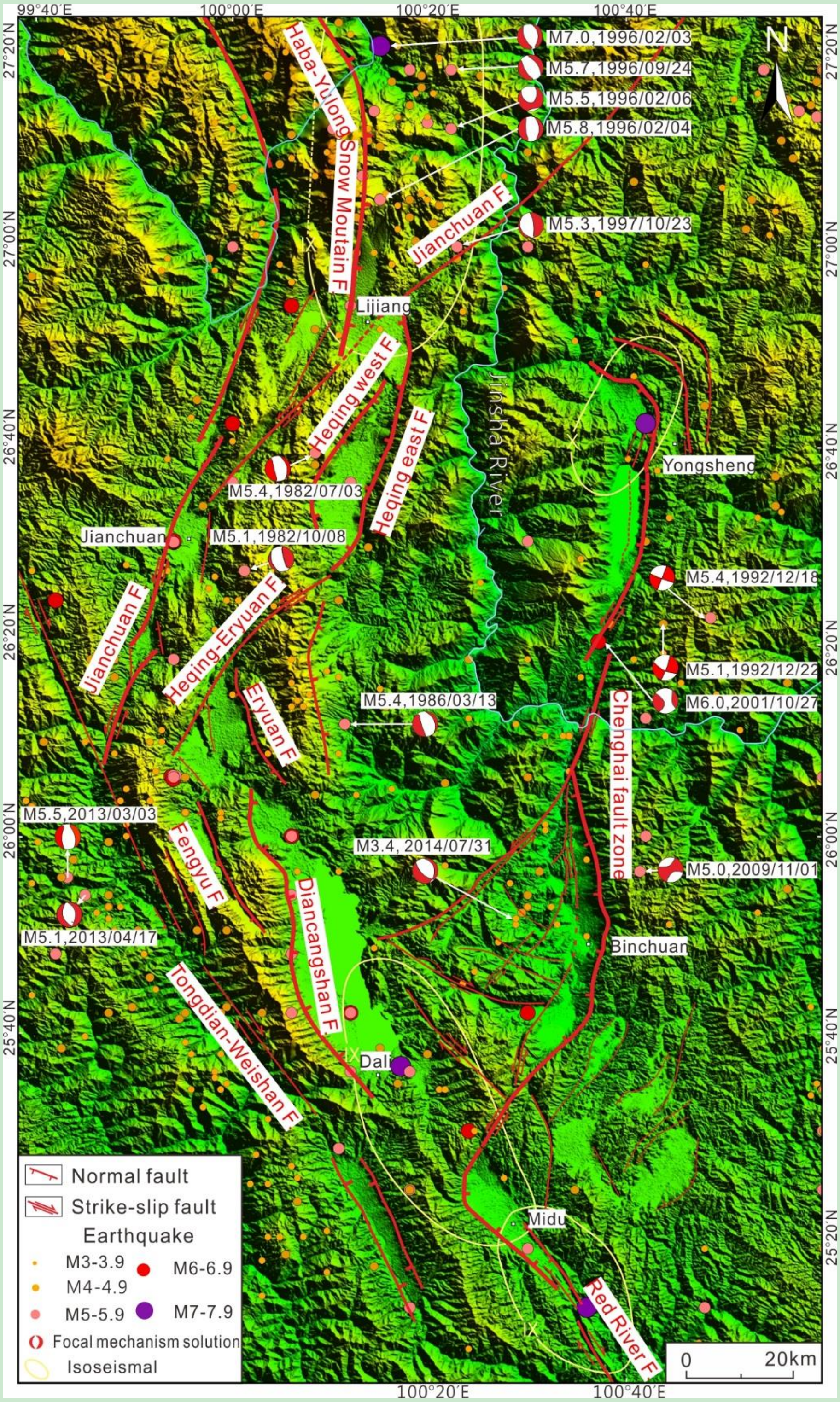

Figure 2. Major active faults and recent seismic events recorded in the Dali fault system, shown on an SRTM 90 m digital elevation model image. Yellow ovals represent the meizoseismal area of large earthquakes (M≥7). Seismic parameters come from China Seismic Information and Mao et al. (2003).

Figure 3. Geological map of the Chenghai fault zone with the segmentation of major faults. Black lines instruction the location of the profile. Abbreviations of fault segments: YS–CHS: the Yongsheng–Chenghai segment, QNS: the Qina segment, BCS: the Binchuan segment, MLPS: the Maolipo segment, MDS: the Midu segment.

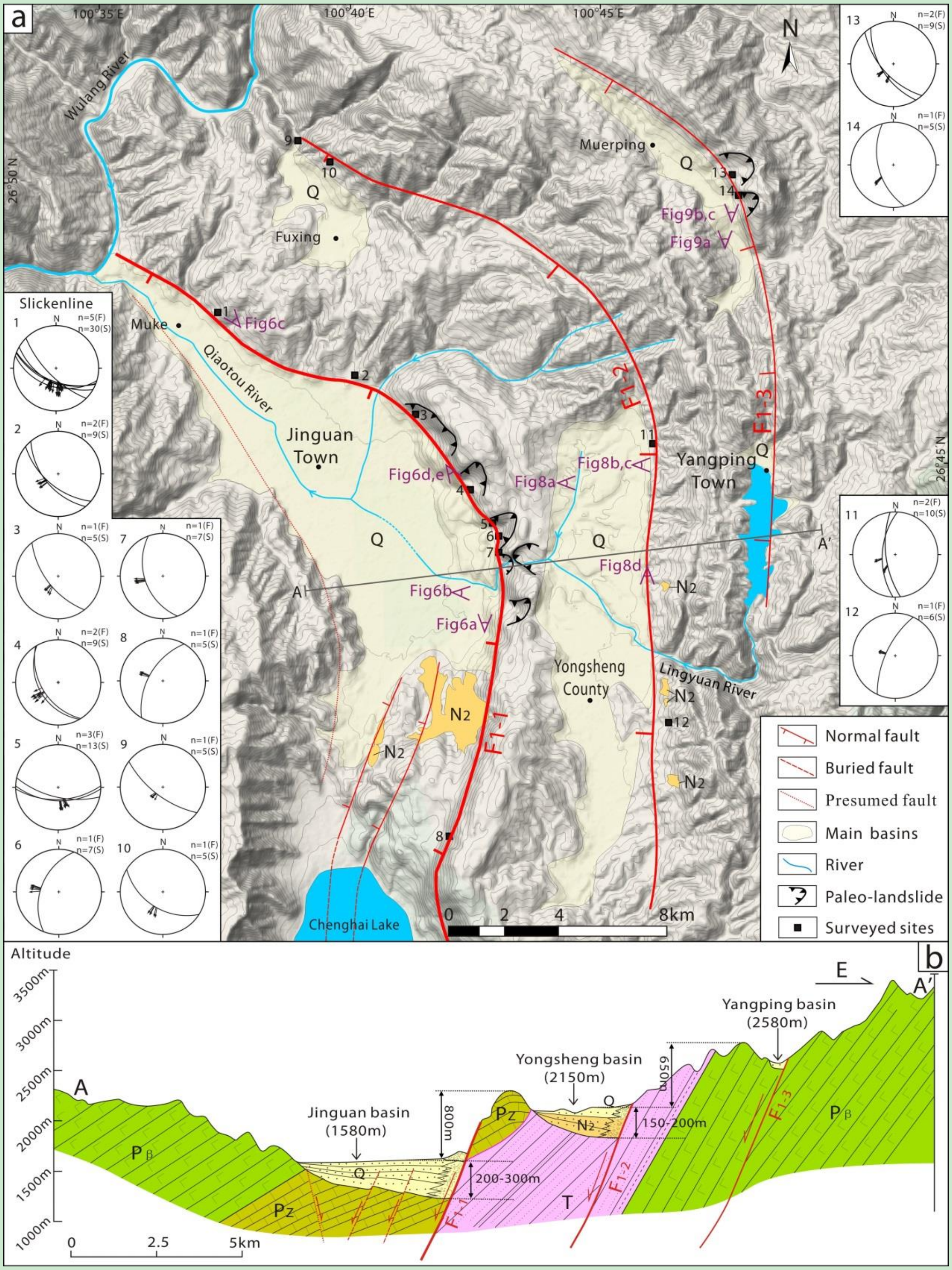

Figure 4. (a) Major active faults in the north section of the Yongsheng–Chenghai segment, show on topographic map, with stereoplots of the collected fault and slickenlines data (Schmidt net, lower hemisphere projection, fault as great circle and slickenlines as arrows). Black squares mark the locations were measured fault kinematic markers during field survey. (b) Geological cross section along profile A–A' (See Figures 2, 4a for location).

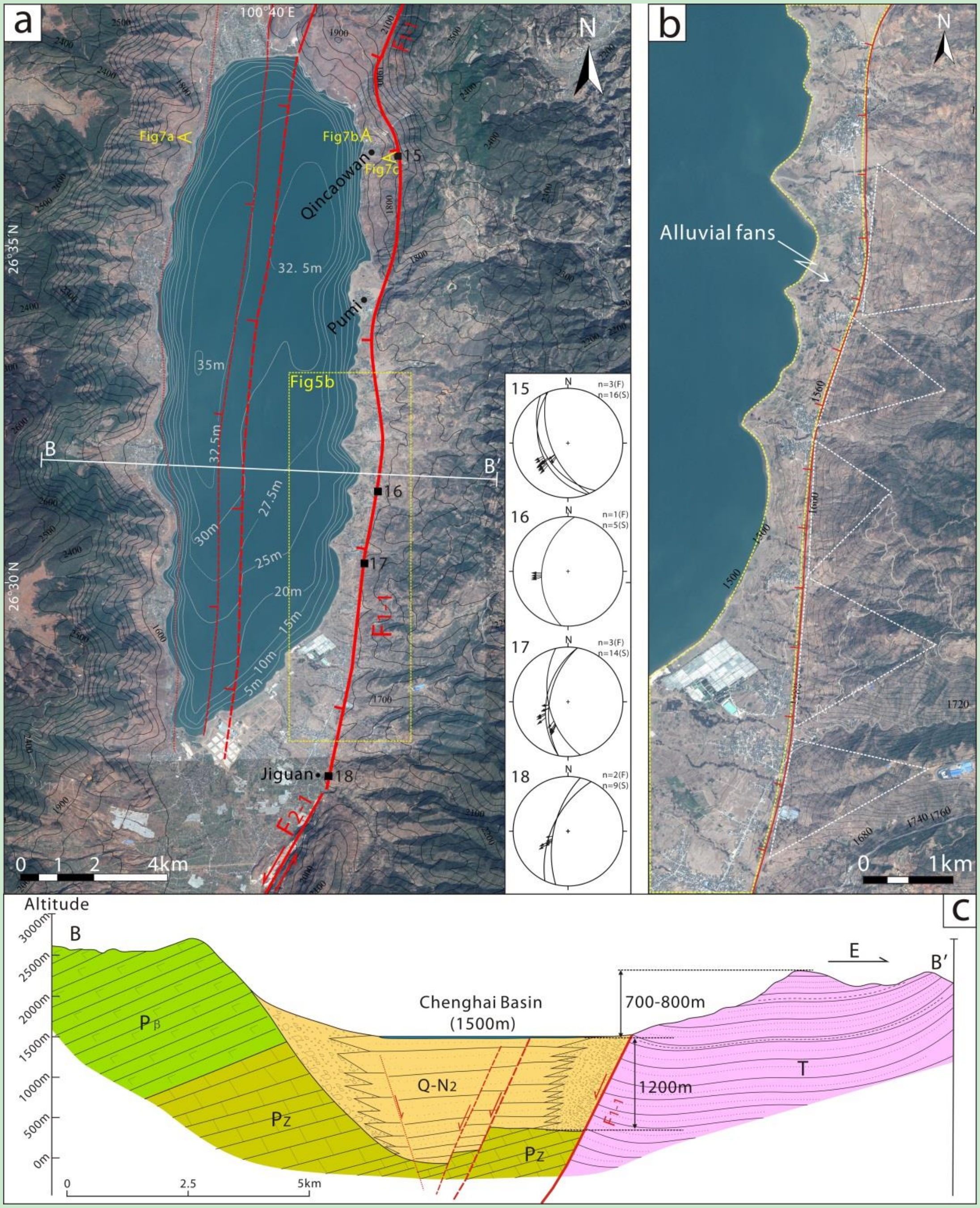

Figure 5. (a) Satellite image of the Chenghai Lake overlaid with topographic and bathometric lines, with stereoplots of the collected fault and slickenlines data. Dotted red line indicates inferred fault traces. Black squares mark the locations were measured fault kinematic markers during field survey. (b) Satellite image showing triangular facets and alluvial fans along the Jinguan–Chenghai fault. (c) Geological section along B–B’ (See Figures 2, 5a for location).

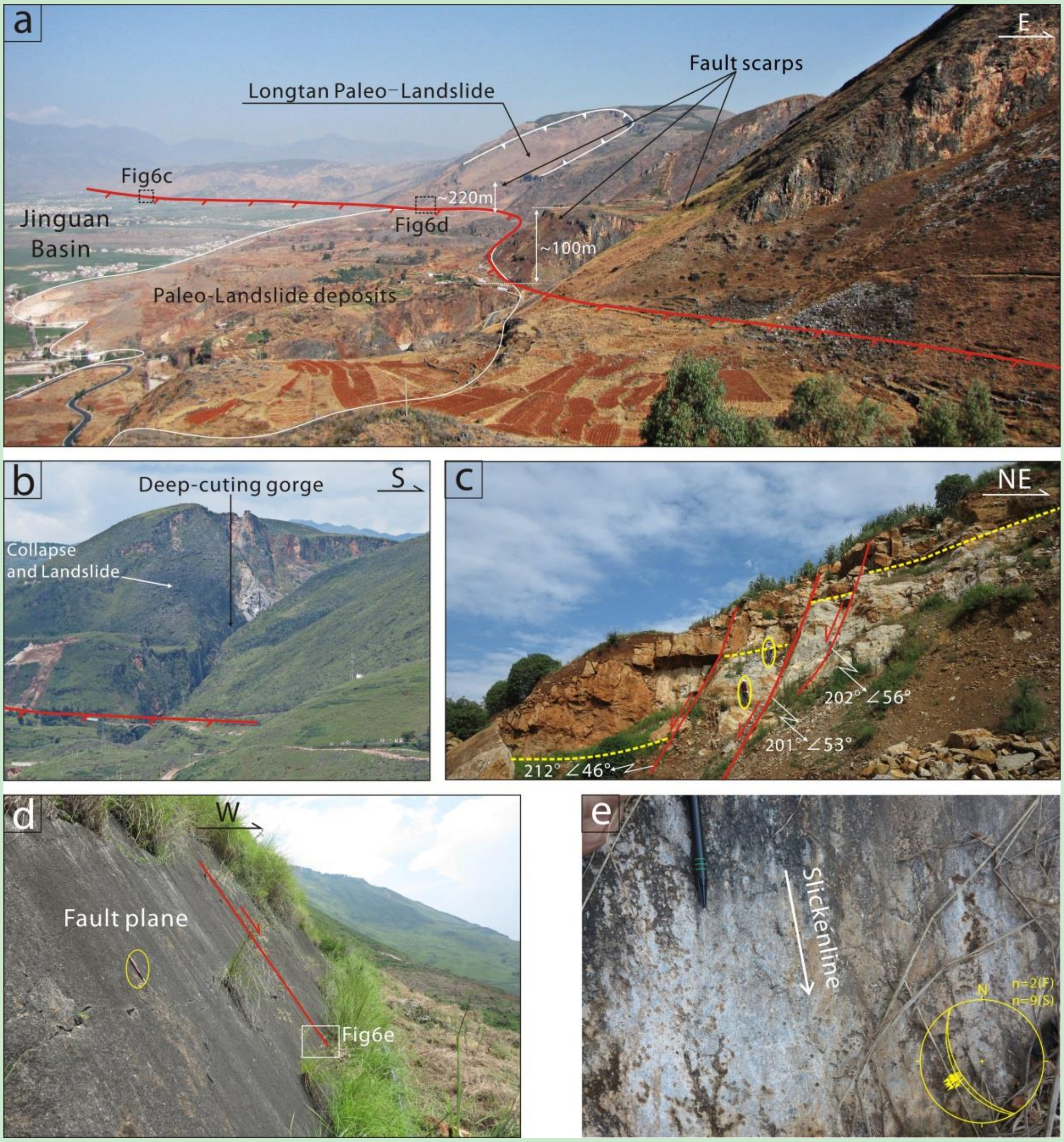

Figure 6. (a) Panoramic view showing labeled fault scarps and paleo–landslides along the Jinguan–Chenghai fault. (b) Distant view showing a deep, narrow gorge within the up thrown footwall of the Jinguan–Chenghai fault. (c) Close–up of the fault showing three stepping normal faults in the fault damage zone. (d) Meter–scale, the most recent fault scarp of the Jinguan–Chenghai fault. (e) Detail view (see Figure 6d), showing a polished fault surface with dip–parallel slickenlines. Lower–right corner is stereoplot of the collected fault and slickenlines data.

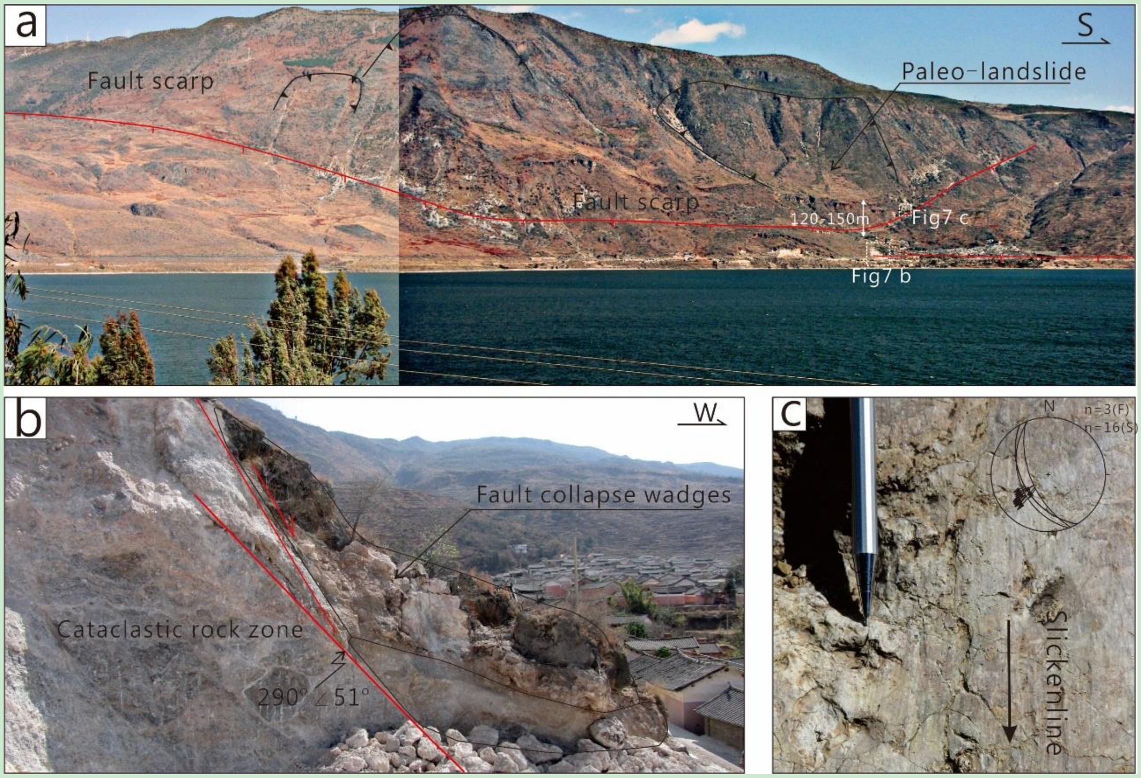

Figure 7. (a) Panoramic view showing the steep fault scarp that forms the eastern boundary of Chenghai basin. (b) Close–up of the fault showing a cataclastic fault zone and collapsed fault wedge exposed in the wall of a quarry. (c) Detail view (see Figure 7a), showing a polished fault surface with dip–parallel slickenlines, upper–right corner is stereoplot of the collected fault and slickenlines data.

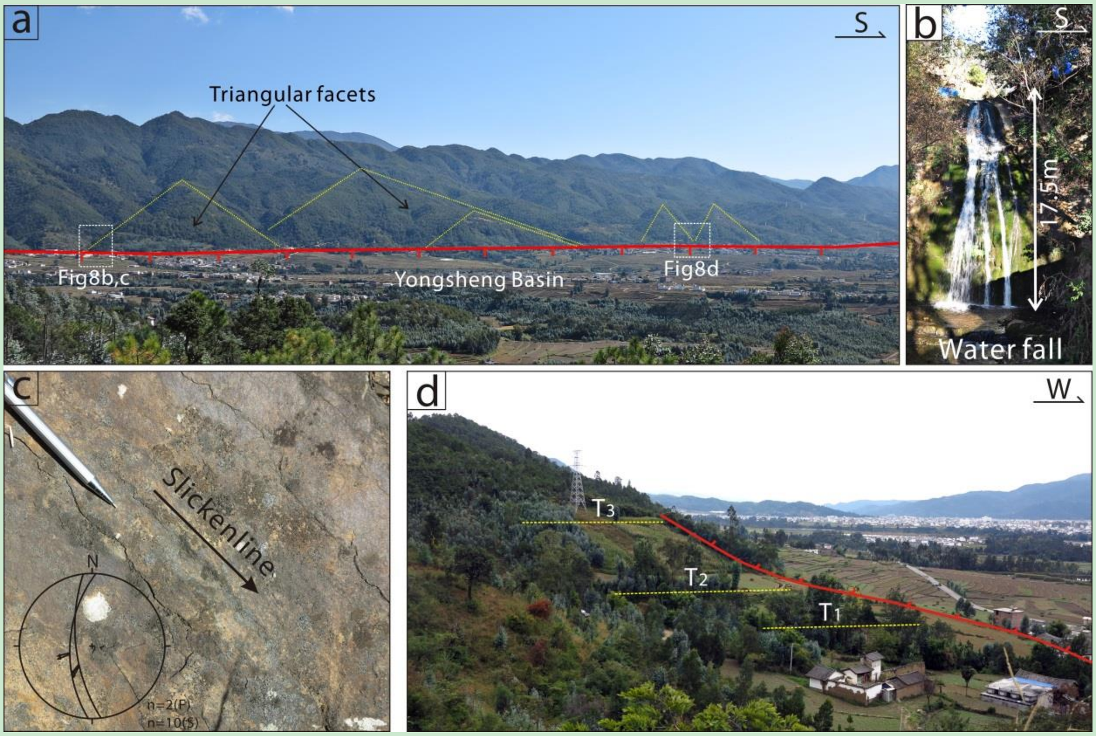

Figure 8. (a) Panoramic view showing well developed triangular facets in Mesozoic sandstone along the Yongsheng fault. (b) Photograph showing a water fall created by vertical displacement of the Yongsheng fault. (c) Detail view (see Figure 8a), showing a polished fault surface with oblique slip slickenlines, lower–left corner is stereoplot of the collected fault and slickenlines data. (d) Photograph showing three–level of river terrace on the footwall of the Yongsheng fault.

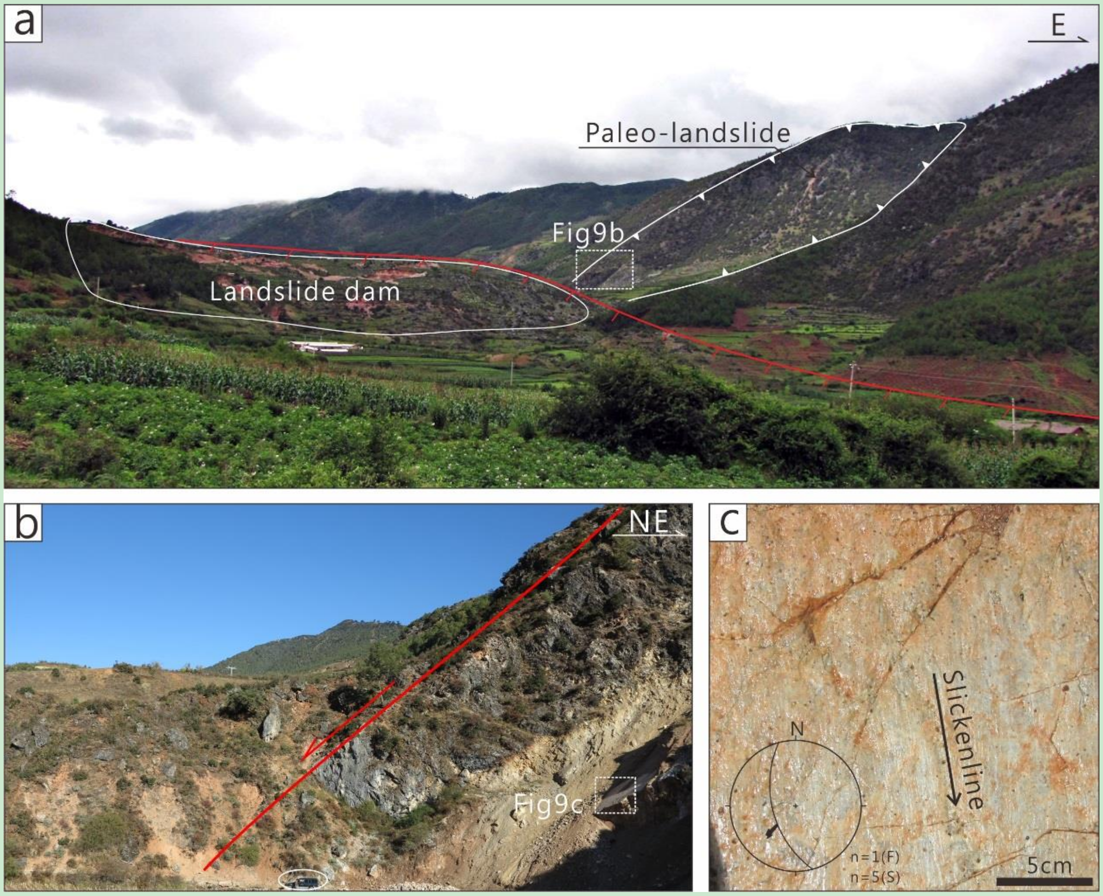

Figure 9. Panoramic view shows linear triangular facets and huge paleo–landslide along the Muerping–Yangping fault. (b) Close view showing the fault forms a boundary between the Permian limestone and landslide deposits. (c) Detail view (see Figure 9b), showing a polished fault surface with almost dip–parallel slickenlines, lower–left corner is stereoplot of the collected fault and slickenlines data.

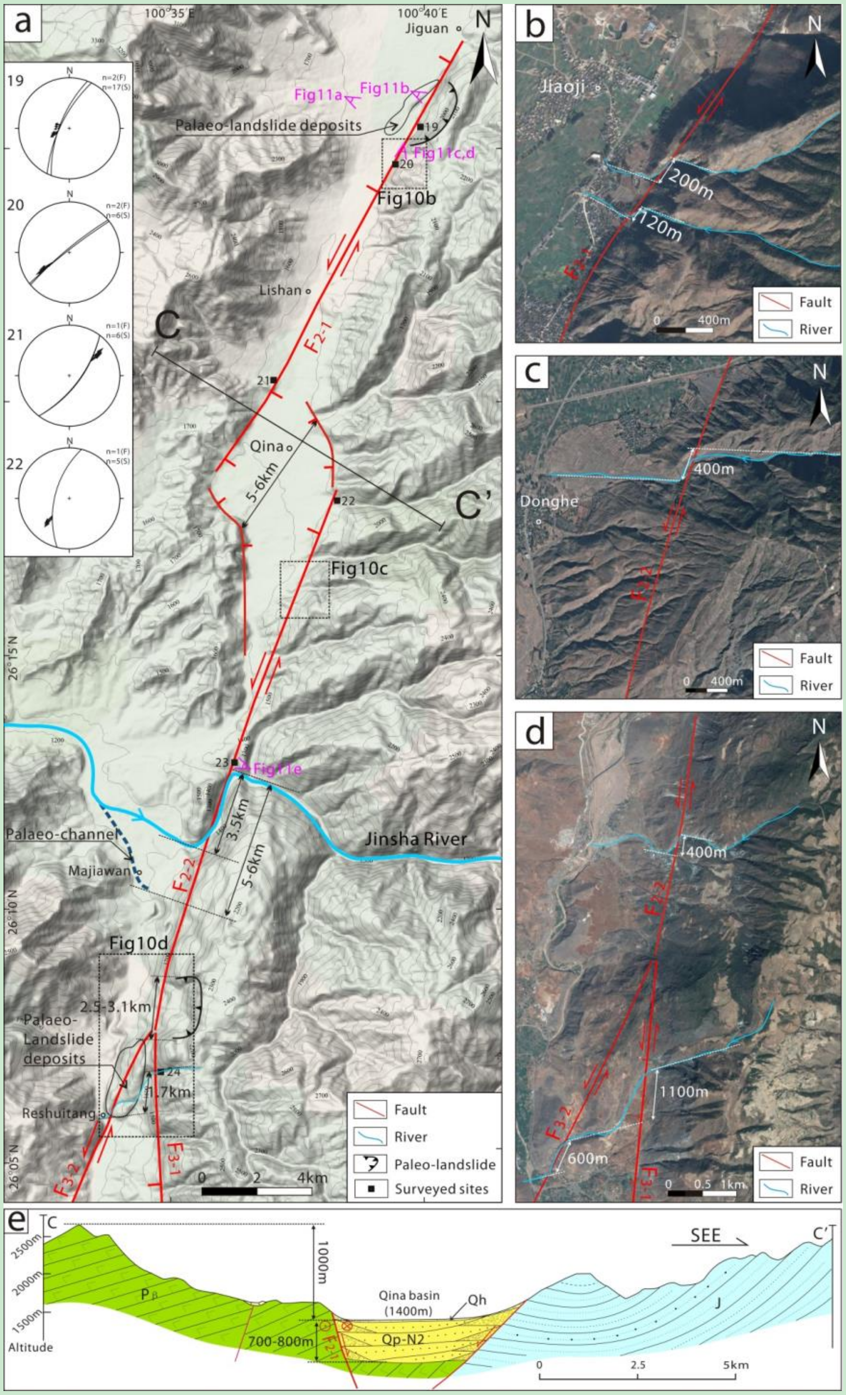

Figure 10. (a) Major active faults in the Qina segment, show on topographic map, with stereoplots of the collected fault and slickenlines data. Black lines with solid triangles indicate the extent of landslides. Black squares mark the locations were measured fault kinematic markers during field survey. (b, c, d) Satellite images showing stream offsets along Qina and Jinjiang fault. (e) Geological cross section along profile C–C' (See Figures 2, 10a for location).

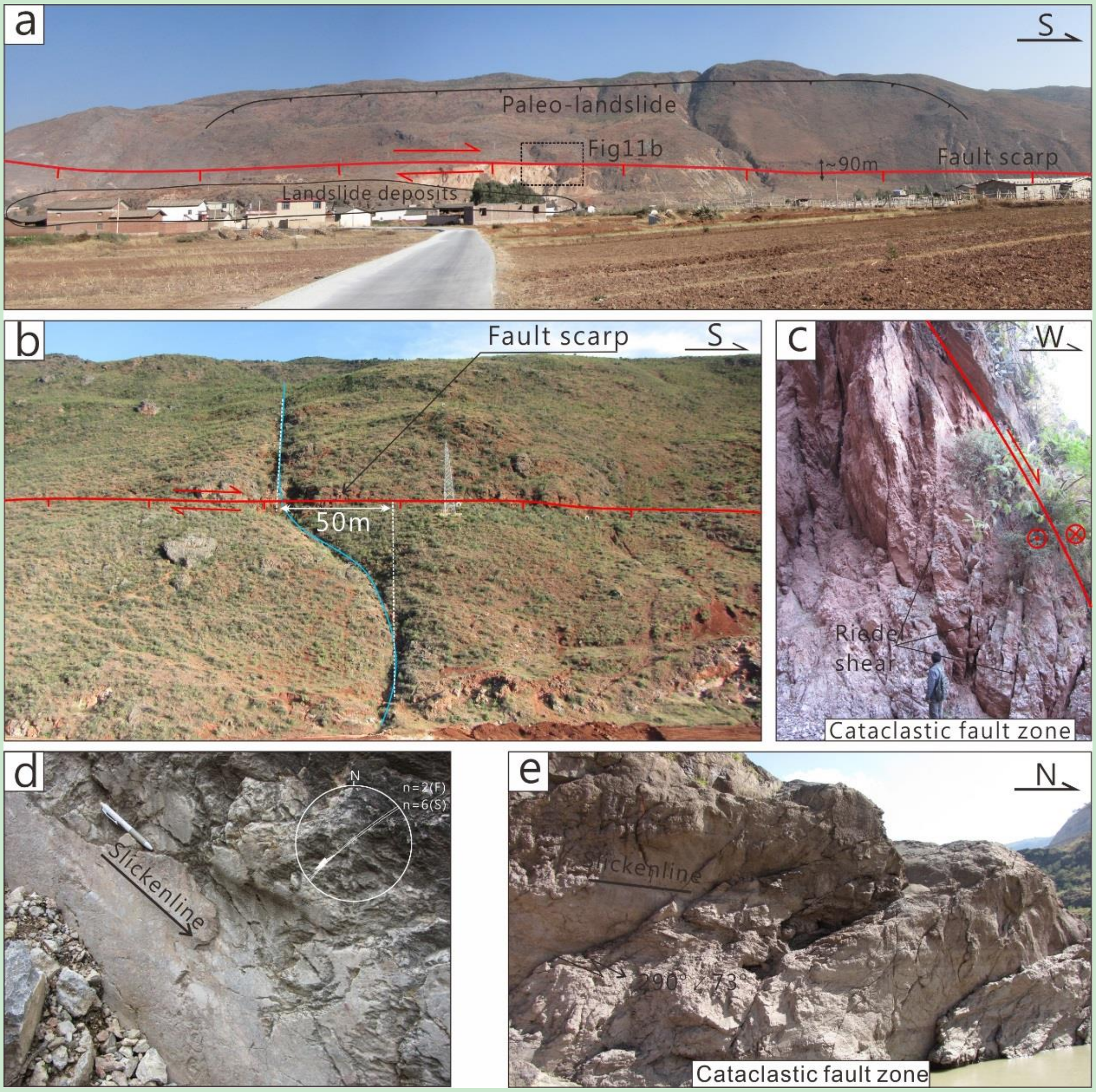

Figure 11. (a) Photograph showing a steep fault scarp along the Qina fault and a paleo–landslide on it. (b) Close view showing a fresh fault scarp left–laterally offsetting a stream as it crosses the Qina fault. (c) Close–up view showing a cataclastic fault zone localizes within the Permian limestone, with development of foliated cataclasites, with kinematic indicator as Riedel shears indicating normal kinematics. (d) Detail view showing a polished fault surface with oblique slip slickenlines, upper–right corner is stereoplot of the collected fault and slickenlines data. (e) Close–up view showing a cataclastic fault zone localizes within the Permian limestone, along the Jinjiang fault.

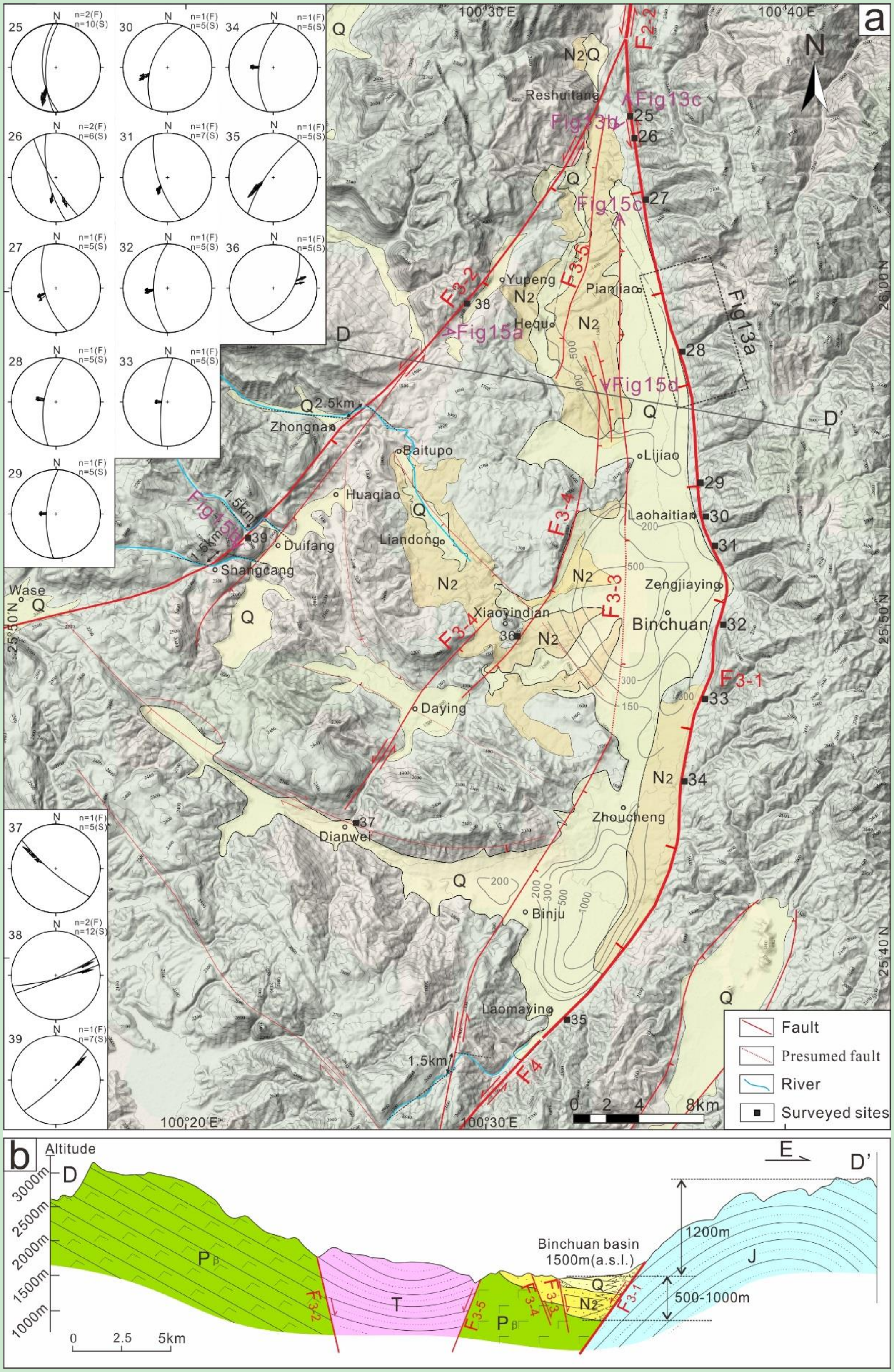
a
b
N
100°30'E
100°40'E
100°20'E
25°50'N
25°40'N
26°00'N
Q
N2
F2-2
F3-1
F3-2
F3-3
F3-4
F3-5
F4
Reshuitang
Yupeng
Pianjiao
Hequ
Zhongnan
Baitupo
Huaqiao
Liandong
Duifang
Shangcang
Wase
Lijiao
Laohaitian
Zengjiaying
Binchuan
Xiaoyindian
Daying
Dianwei
Zhoucheng
Binju
Laomaying
Fig13a
Fig13b
Fig13c
Fig15a
Fig15b
Fig15c
Fig15d
2.5km
1.5km
Fault
Presumed fault
River
Surveyed sites
0 2 4 8km
Altitude
D
D'
E
Binchuan basin
1500m(a.s.l.)
1200m
500-1000m
J
T
Pβ
3000m
2500m
2000m
1500m
1000m
0 2.5 5km

Figure 12. (a) Major active faults in the Binchuan segment, show on topographic map, with stereoplots of the collected fault and slickenlines data. Black squares mark the locations were measured fault kinematic markers during field survey. Grey lines represent isopach of the thickness of Late Cenozoic sediments (from hydrogeological map). (b) Geological cross sections along D–D’ (See Figures 2, 12 for location).

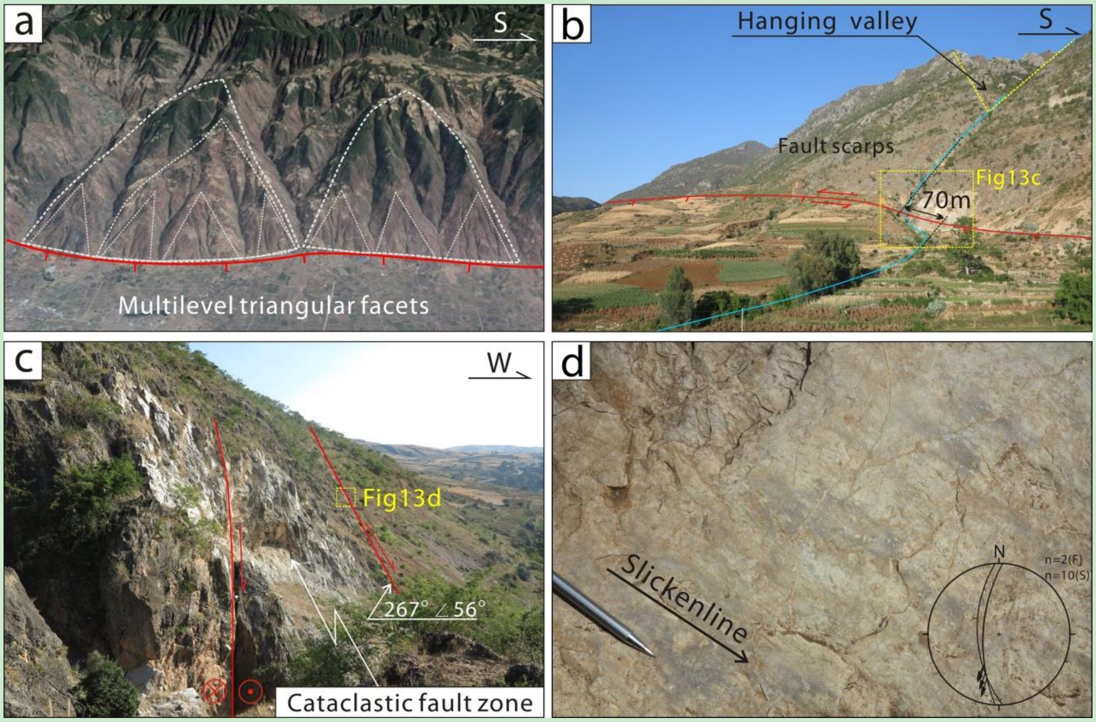

Figure 13. (a) Google earth image showing three–level triangular facets along the Binchuan fault. (b) Close view showing a fault scarp with hanging valley and left lateral offset stream on it. (c) A close–up of cataclastic fault zone localizes within the Permian limestone, with development of foliated cataclasites. (d) Detail view showing a polished fault surface with oblique slip slickenlines, lower–right corner is stereoplot of the collected fault and slickenlines data.

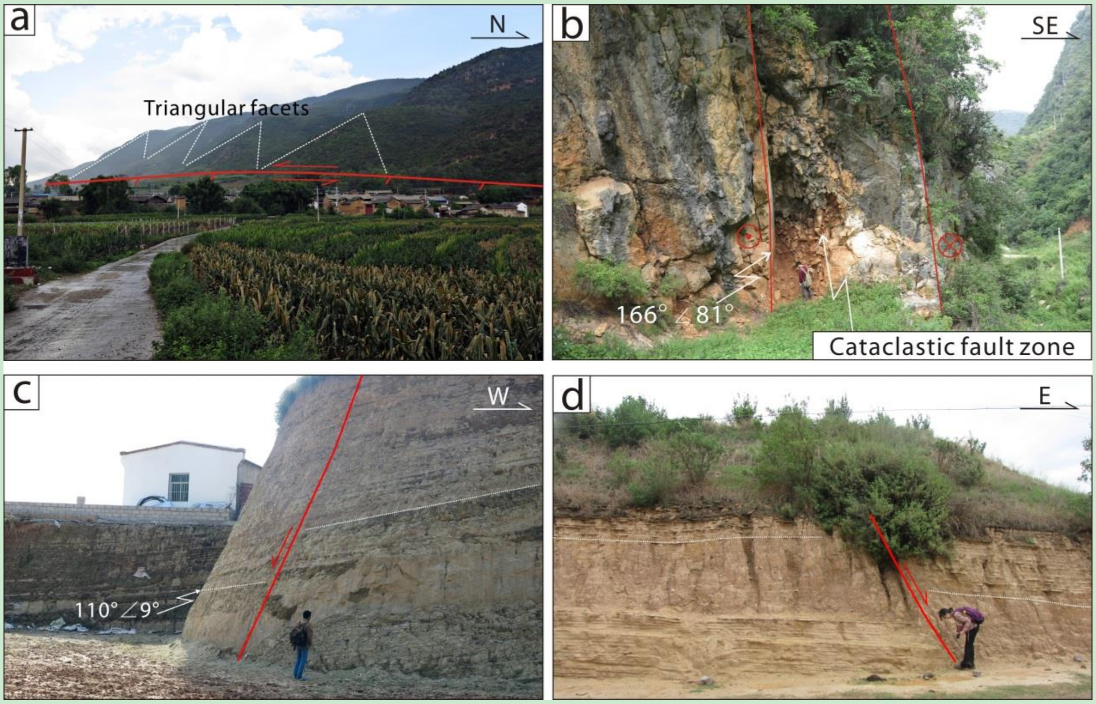

Figure 14. (a) A overview look at the triangular facets along the Shangcang–Yupeng fault. (b) A close-up showing a cataclastic fault zone localizes within the Permian limestone. (c) Photograph showing a small normal fault in late Cenozoic lacustrine strata. (d) A close-up showing the Pianjiao–Daying fault cuts through late Cenozoic strata.

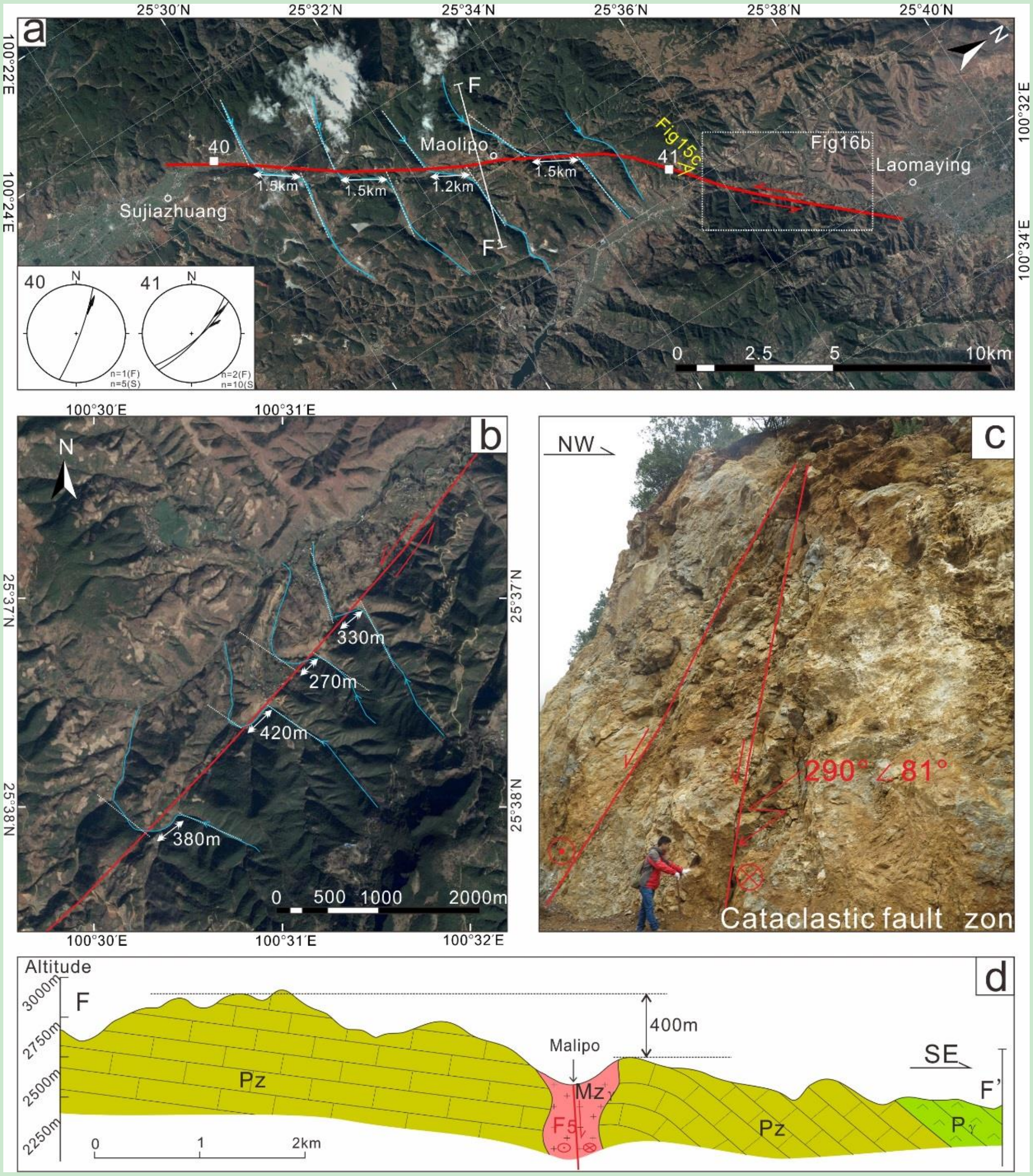

Figure 15. (a) Satellite image shows the distribution of the Maolipo fault, with stereoplots of the collected fault and slickenlines data. Red lines indicate the location of the fault, blue lines show the streams offset by sinistral slip fault. Black squares mark the locations were measured fault kinematic markers during field survey. (b) Satellite image shows young streams are offset by sinistral slip fault at the north tip of the Maolipo fault. (c) A close-up showing a cataclastic fault zone localizes within the Devonian limestone. (d) A geological profile of Maolipo segment (see figures 2, 15a for location).

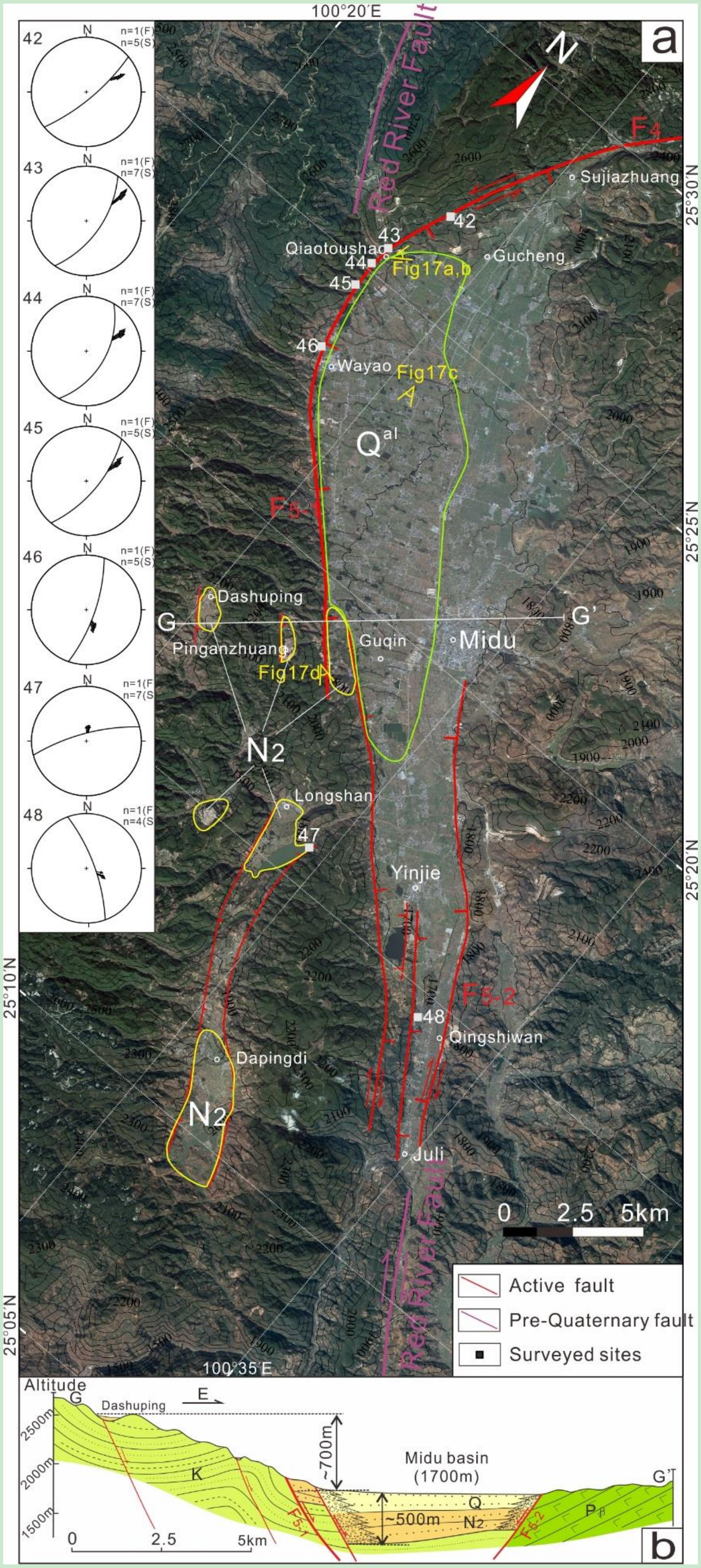

Figure 16. (a) Satellite image shows major faults of the Midu segment, with stereoplots of the collected fault and slickenlines data. Black squares mark the locations were measured fault kinematic markers during field survey. (b) A geological cross section of the Midu basin (see figures 2, 16a for location).

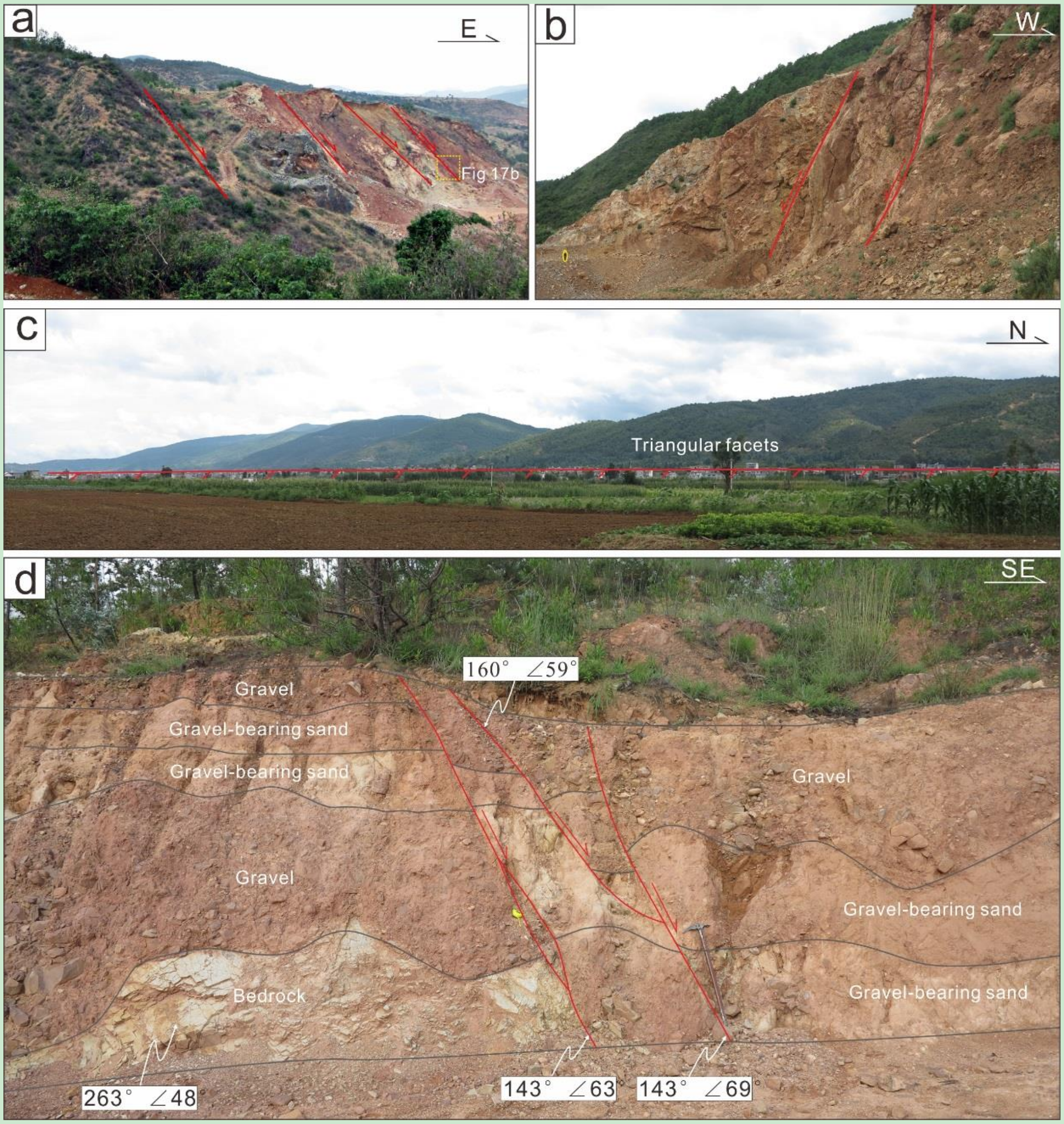

Figure 17. (a) Photographs showing a fault zone with multiple parallel fault planes in Permian limestone. (b) Close view of the rightmost fault in figure 17a. (c) Distant view showing liner triangular facets along the Midu fault. (d) Photographs showing the Midu fault cut through the Cretaceous strata and Pliocene deposits rest on it.

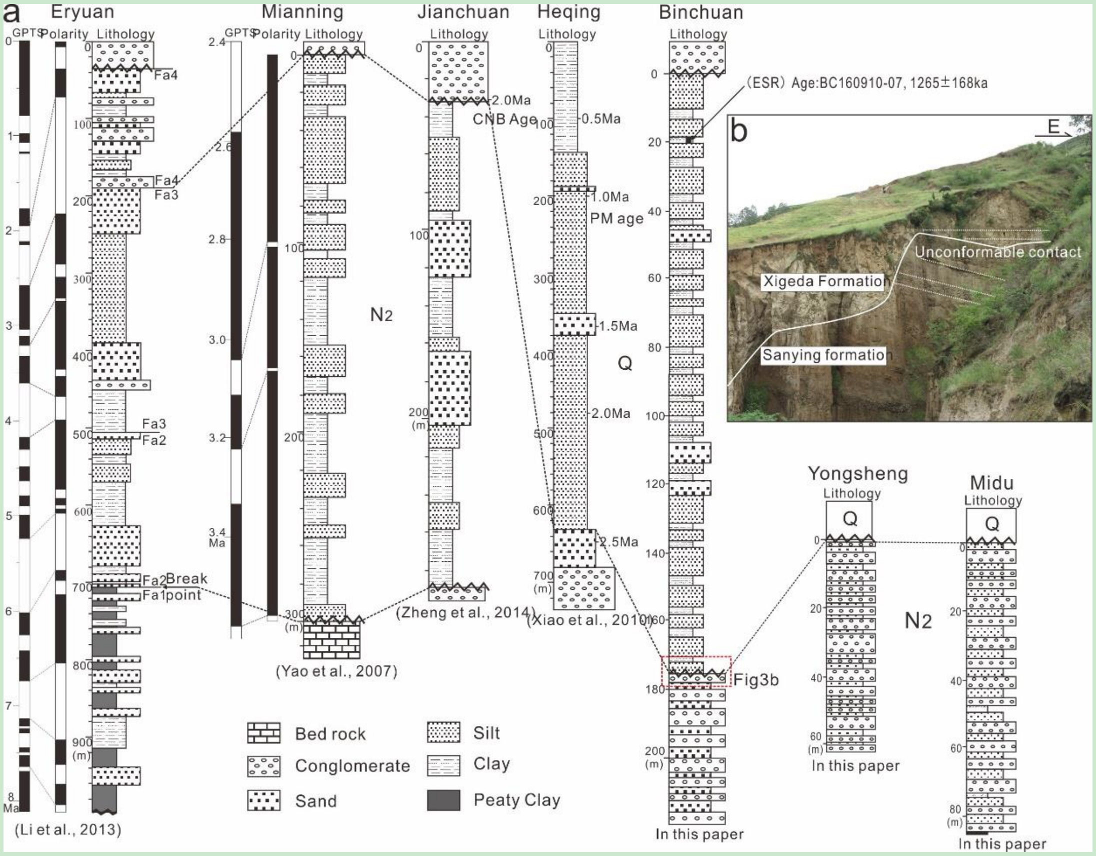

Figure 18. (a) Stratigraphic correlation of the Sanying Formation and Quaternary lacustrine deposition overlying unconformity covered above the Sanying Formation, in Dali fault system and its adjacent area. (b) Photographs showing Quaternary lacustrine deposition overlying unconformity covered above the Sanying Formation.

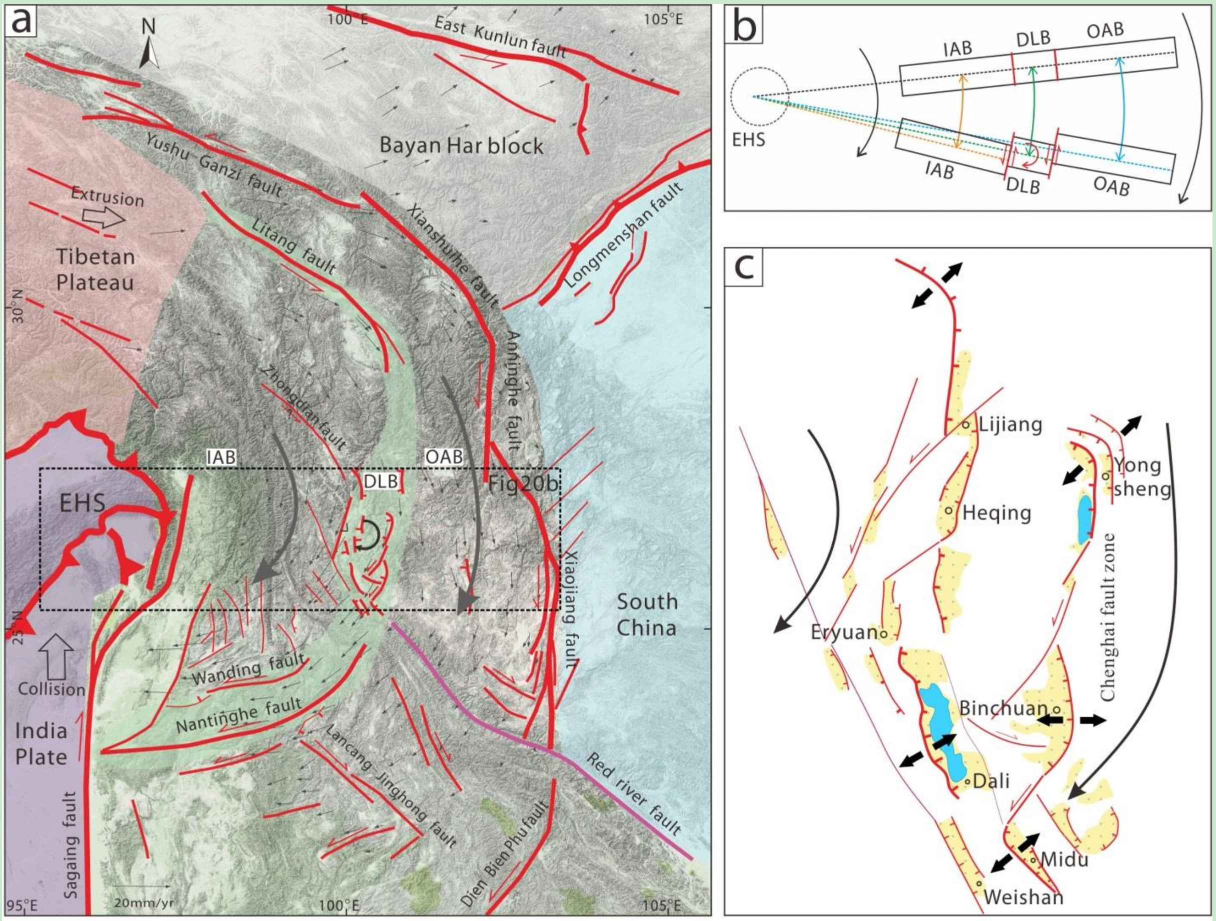

Figure 19. (a) The present active tectonic framework on the southeastern margin of the Tibetan Plateau. Red lines represent active faults and purple lines represent Pre–Quaternary faults. Abbreviations, EHS: eastern Himalayan syntaxis, IAB: the inner arcuate belt, OAB: the outer arcuate belt, DLB: Dali block. (b, c) The mechanism of clockwise rotation appeared on the Dali block.

Table 1. Main earthquakes parameters (M≥5) along the Chenghai fault zone and earthquakes (M≥7) in Dali fault system.

Time	Lat	Lon	M	SF*
1515/06/27	26.7	100.7	7.8	Jinguan–Chenghai fault
1623/05/04	25.5	100.4	6.3	Maolipo fault
1652/07/13	25.2	100.6	7.0	Midu fault
1803/02/02	25.7	100.5	6.3	Pianjiao–Binju fault
1925/04/16	25.3	100.5	5.0	Midu fault
1959/03/30	26.0	100.7	5.5	Binchuan fault
1959/04/26	26.2	100.7	5.8	Qina fault
1992/12/18	26.4	100.6	5.4	Qina fault
1992/12/22	26.4	100.6	5.1	Qina fault
2001/10/27	26.2	100.6	6.0	Qina fault
2009/11/02	25.9	100.7	5.0	Binchuan fault
1925/3/16	25.7	100.4	7.0	DCEF
1996/2/3	27.2	100.3	7.0	HB–YLF

Seismic parameters come from China Seismic Information and Mao et al. (2003). SF*= seismogenic faults. See figure 2 for faults Abbreviation.

Table 2. The displacement and slip rate of the Chenghai fault zone

Fault Name	No.	VD* (m)	HD* (m)	Dip–slip rate (mm/yr)	Left–slip rate (mm/yr)
Jinguan–Chenghai Fault	F_{1-1}	1000–2000	–	0.17–0.4	–
Yongsheng Fault	F_{1-2}	800–850	–	0.13–0.17	–
Muerping–Yangping Fault	F_{1-3}	400–500	–	0.07–0.1	–
Jinjiang Fault	F_{2-2}	1700–1800	5000－6000	0.28–0.36	0.83–1.2
Binchuan Fault	F_{3-1}	1700–2200	–	0.28–0.44	
Shangcang–Yupeng Fault	F_{3-2}	800	2500	0.13–0.16	0.41–0.5
Maolipo Fault	F_4	400	1500	0.07–0.08	0.25–0.3
Midu Fault	F_{5-1}	1200	–	0.20–0.24	–

VD*: Vertical displacement, HD*: Horizontal displacement.